UNIVERSITÀ DEGLI STUDI FIRENZE

FLORE
Repository istituzionale dell'Università degli Studi di Firenze

The Jurassic association of backarc basin ophiolites and calkalcaline volcanics in the Guevgueli complex (Northern Greece: implication for

Questa è la Versione finale referata (Post print/Accepted manuscript) della seguente pubblicazione:

Original Citation:

The Jurassic association of backarc basin ophiolites and calkalcaline volcanics in the Guevgueli complex (Northern Greece: implication for the evolution of the Vardar Zone) / E.Saccani ; V.Bortolotti ; M.Marroni; L.Pandolfi; A.Photiades; G. Principi. - In: OFIOLITI. - ISSN 0391-2612. - STAMPA. - 33(2):(2008), pp. 209-227.

Availability:

This version is available at: 2158/343367 since:

Terms of use:

Open Access

La pubblicazione è resa disponibile sotto le norme e i termini della licenza di deposito, secondo quanto stabilito dalla Policy per l'accesso aperto dell'Università degli Studi di Firenze (https://www.sba.unifi.it/upload/policy-oa-2016-1.pdf)

Publisher copyright claim:

(Article begins on next page)

12 October 2024

THE JURASSIC ASSOCIATION OF BACKARC BASIN OPHIOLITES AND CALC-ALKALINE VOLCANICS IN THE GUEVGUELI COMPLEX (NORTHERN GREECE): IMPLICATION FOR THE EVOLUTION OF THE VARDAR ZONE

Emilio Saccani*,✉, Valerio Bortolotti, Michele Marroni***,°, Luca Pandolfi***,°, Adonis Photiades°°** and **Gianfranco Principi**,°**

* *Dipartimento di Scienze della Terra, Università di Ferrara, Italy.*
** *Dipartimento di Scienze della Terra, Università di Firenze, Italy.*
*** *Dipartimento di Scienze della Terra, Università di Pisa, Italy.*
° *Istituto di Geoscienze e Georisorse, CNR, Italy.*
°° *Department of General Geology and Geological Mapping, Institute of Geology and Mineral Exploration (IGME), Athens, Greece.*
✉ *Corresponding author, e-mail: sac@unife.it*

Keywords: *Ophiolite, backarc basin basalt, calc-alkaline, Jurassic, Vardar Zone, Hellenides. Greece.*

ABSTRACT

The Middle-Late Jurassic Guevgueli Complex (Greek Macedonia) represents one of the main ophiolitic complexes of the Vardar Zone and has been subdivided into two distinct sub-units, that are the East and West Guevgueli, both including intrusive and volcanic sequences crosscut by several dykes. The Guevgueli Complex is intruded by the Fanos Granite and, together with this, is sandwiched, through a north-south striking thrust zone, between the Serbo-Macedonian Massif, to the east, and the Paikon Unit, to the west. Intrusive rocks are represented mainly by gabbros showing both cumulitic and isotropic textures and very subordinate ultramafic cumulates, Fe-gabbros, and diorites. Mineralogically and chemically, they are very similar to high-Ti, mid-ocean ridge-type gabbros, having high contents of Ti and V, and very low contents of incompatible elements. However, many isotropic gabbros show some subduction-related imprinting testified by Nb, Zr, and Ti relative depletion and light rare element (LREE) enrichment with respect to heavy rare earth elements (HREE). Incompatible elements and rare earth elements analyses carried out on volcanic, and subvolcanic rocks from both East and West Guevgueli indicate that two different rock-types can be identified within the volcanic sequences. They are: (1) calc-alkaline (CAB) rocks ranging from basalt to basaltic andesite, andesite, dacite, and rhyolite represented by lavas and dykes; (2) back-arc basin basalts (BABB) occurring as pillow lavas, as well as dykes crosscutting High-Ti gabbros and CAB volcanic series. CAB rocks show marked depletion in Nb, Ta Ti and enrichment in LREE and Th, which point out for their generation in a volcanic arc setting that can be most likely correlated with the development of the Paikon volcanic arc onto the Serbo-Macedonian continental realm. BABB rocks show many similarities with mid-ocean ridge basalts (MORB), such as marked Fe, Ti, V enrichment from less fractionated to fairly fractionated rocks, relatively high Ti, P, Y contents, and significant Nb depletion. However, they show higher Th/Ta and LREE/HREE ratios compared with MORBs. Such characteristics are commonly interpreted as a typical supra-subduction zone chemical imprinting, which can be correlated with the injection of a MORB-type mantle source into the sub-arc mantle wedge. In addition, BABB volcanic and subvolcanic rocks display co-magmatic relationships with the associated gabbros. So, the Guevgueli ophiolites can be regarded as representative of an ensialic back-arc basin located between the Paikon Volcanic arc and the continental margin of the Serbo-Macedonian Massif. In this framework, the close association in the Guevgueli Complex of coeval oceanic and continental arc magmatic rocks can be explained as the result of the opening of the back-arc basin mainly controlled by transtension leading to complex geometry of boundaries between the volcanic arc and the oceanic basin.

INTRODUCTION

The Dinaric-Hellenic belt is an Alpine collisional chain derived from the Mesozoic to Tertiary convergence between the Eurasia and Adria Plates. Several models about the evolution of this collisional belt have been proposed in the past (e.g., Şengör and Yılmaz, 1981; Robertson and Dixon, 1984; Robertson et al., 1996; Stampfli and Borel, 2002; Brown and Robertson, 2004; Bortolotti et al., 2005; Smith, 2006; Sharp and Robertson, 2006), most of them focused on the geodynamic history from Jurassic to Early Tertiary time span. These models show significant differences about the number and the location of the oceanic basins, whose remnants are nowadays preserved in the numerous ophiolite sequences cropping out from Croatia and Serbia to Greece. In order to provide useful constraints for the proposed geodynamic model, one of the fundamental tools is represented by the geochemical affinity of ophiolites. Actually, ophiolites developed in different geodynamic settings including mid-ocean ridge, intra-oceanic island arc, back-arc, and fore-arc, and their geochemical features can unambiguously identify their origin. In Greece, one the matter of debate concerns the geodynamic significance of the Upper Jurassic Guevgueli ophiolites sequence, belonging to the Vardar Zone (Fig. 1a) and strictly associated to Upper Jurassic granites (Fig. 1b) derived from lower crustal melts (Sariç et al., 2008).

The main purpose of this paper is thus to discuss the geochemical and petrogenetic characteristics of the Guevgueli ophiolitic and the associated arc-type rocks from the Guevgueli Complex, in order to decipher their original tectono-magmatic setting.

GEOLOGICAL SETTING

Regional geological setting and previous work

The evolution of the Dinaric-Hellenic belt started with a rifting stage developed during the Early Triassic time along

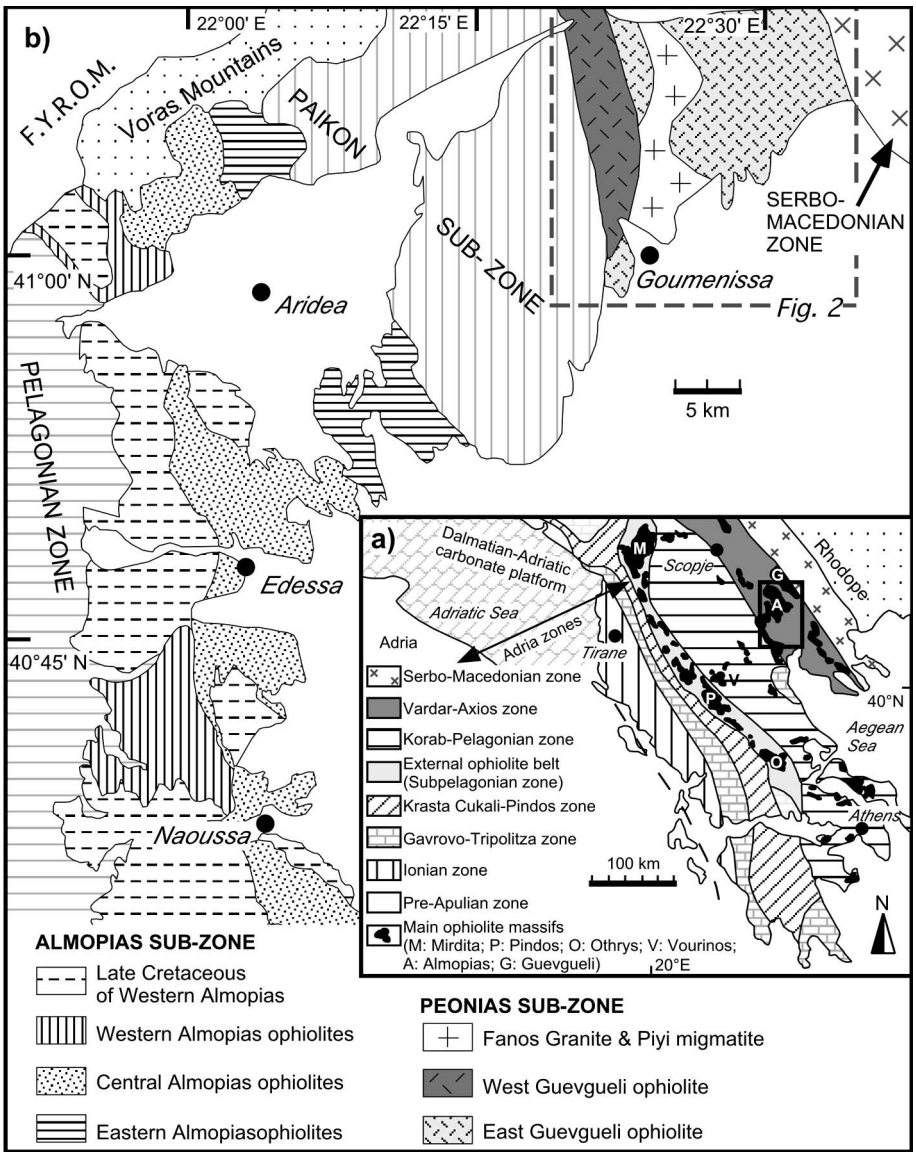

Fig. 1 - a): Tectono-stratigraphic zones of the Albanide-Hellenide belt (modified from Saccani et al., 2004 and Robertson et al., 2008); b): geological sketch-map of the Vardar Zone in the northern Greece (modified from Pe-Piper and Piper, 2002 and Saccani et al., 2008). Box in Fig. 1a indicates the area expanded in Fig. 1b; dashed box in Fig. 1b is expanded in Fig. 2.

the northern margin of Gondwanaland (Pamić et al., 2002; Bortolotti et al., 2004; 2005; Brown and Robertson, 2004). The rifting process, characterized by thick sedimentation of sin-rift deposits and alkaline magmatism, evolved during the Middle to Late Triassic to the oceanic opening, as suggested by recent findings of mid-ocean ridge-type ophiolites of Triassic age in Albania (Bortolotti et al., 2004; 2006), as well as in Greece (Bortolotti et al., 2003; Saccani et al., 2003; Bortolotti et al., 2008, this volume). A development of a wide basin characterized by mid-ocean ridge oceanic lithosphere resulted in the Early Jurassic from the following spreading and drifting phases (Papanikolaou, 1984; Robertson and Dixon, 1984; Mountrakis, 1984; Dercourt et al., 1993; Bortolotti et al., 1996; 2004; 2005; Robertson et al., 1996; Michard et al., 1998; Stampfli and Borel, 2002; Pamić et al., 2002; Saccani et al., 2004; Brown and Robertson, 2004; Smith, 2006; Sharp and Robertson, 2006). This oceanic basin, with (e.g., Jones and Robertson, 1991; Shallo, 1992; Doutsos et al., 1993; Beccaluva et al., 1994; Ross and Zimmermann, 1996; Robertson and Shallo, 2000; Kodra et al., 2000; Dilek et al., 2007) or without (e.g., Bernoulli and Laubscher 1972; Zimmermann, 1972; Vergély, 1976; Jacobshagen et al., 1978; Collaku et al., 1992, Schermer, 1993; Bortolotti et al., 1996; 2002; 2004) a micro-continent inside, was located between the Adria and Eurasia continental margins. The convergence began during the Early Jurassic, with the development of an intra-oceanic subduction followed by the formation of new oceanic lithosphere in the supra-subduction basin. As a consequence of convergence, obduction resulted in the emplacement of oceanic lithosphere slices onto the continental margins of the Adria Plate during the Middle to Late Jurassic times (Mercier, 1966; Vergély, 1984; Ricou and Godfriaux, 1991; Robertson et al., 1996; Michard et al., 1998; Pamić et al., 2002; Bortolotti et al., 2004; 2005; Saccani et al., 2004; Brown and Robertson, 2004; Smith, 2006; Sharp and Robertson, 2006). The convergence between Adria and Eurasia led to the continental collision, whose age (Late Jurassic/Early Cretaceous vs. Early Tertiary) is still matter of debate (see Bortolotti and Principi, 2005 and Bortolotti et al., 2005 for a complete review). The continental collision was also characterized by the emplacement of calc-alkaline granitoids, which along the Greek geotraverse are mainly of Late Jurassic age (Anders et al., 2005, and quoted references).

This long-lived geodynamic evolution produced the present-day structural pattern of the Dinaric-Hellenic belt, which consists of an assemblage of NW-SE to N-S trending zones, corresponding to the modern concept of terranes (see

discussion in Bortolotti et al., 2004). Each zone consists of an assemblage of variably deformed and metamorphosed tectonic units of oceanic and/or continental origin. Along the Albanian-Greek transect of the Dinaric-Hellenic belt four main zones can be identified. These zones correspond, from west to east, to (Fig. 1a): 1 - The Deformed Adria Zones, 2 - the External Ophiolite belt (Subpelagonian zone), 3 - the Pelagonian Zone and the 4 - the Vardar Zone. These zones are bounded to the west by the undeformed Adria Zone, today located in the Adriatic Sea, and to the east by the Serbo-Macedonian-Rhodope Massif, generally regarded as part of the margin of the Eurasia Plate.

On the whole, the sequences of the Deformed Adria Zones are characterized by unmetamorphosed sedimentary sequences, including Triassic to Paleocene neritic and pelagic carbonate sequences topped by widespread Upper Cretaceous to Miocene siliciclastic turbiditic deposits. The age of inception of the flysch deposition, which ranges from Late Cretaceous in the Pindos zone to the Miocene in the Ionian Zone, is regarded as an evidence of the westward migration of the deformation across the continental margin of the Adria Plate. Eastward, the Deformed Adria Zones are thrust by the External Ophiolite belt (Fig. 1a), characterized by ophiolites ranging in age from Triassic to Jurassic. This nappe includes a stack of ophiolitic units showing at their base a sub-ophiolite mélange (Bortolotti et al., 2004). The geological evidences suggest an emplacement of the ophiolites onto the Adria continental margin during the Late Jurassic (Vergély, 1984; Michard et al., 1984; Robertson et al., 1991; Bortolotti et al., 2005).

By contrast, the Pelagonian zone is represented by an assemblage of tectonic units consisting of a pre-Alpine basement covered by a Permian to Lower Triassic siliciclastic deposits followed by Middle Triassic to Upper Jurassic carbonates. The Pelagonian Units are thrust by the units belonging to the Vardar Zone.

The Vardar Zone, located west to the Serbo-Macedonian Massif (Fig. 1a), is represented by a composite assemblage of continental- and oceanic-derived units, also including Triassic/Jurassic ophiolites (Mercier, 1966; Mercier et al., 1975; Bébien et al., 1994; Brown and Robertson, 2004). The latter represent the Internal Ophiolite belt of the Dinaric-Hellenic chain. In Greece, the Vardar Zone is divided into three main sub-zones (Fig. 1b), which are (from west to east): the Almopias, Paikon, and Peonias (also reported as Guevgueli) (Mercier, 1966).

In the Almopias sub-zone several units consisting of Jurassic and subordinate Triassic ophiolite sequences and related sedimentary covers can be recognized (e.g., Stais et al., 1990; Pe-Piper and Piper, 2002). According to Saccani et al. (2008), the units from the western and central Almopias consist of ophiolite mélanges where harzburgitic mantle tectonites are associated to magmatic rocks, which include mid-ocean ridge basalt (MORB), low-Ti tholeiite (IAT), and very low-Ti boninite varieties. These sequences are unconformably covered by Upper Jurassic - Lower Cretaceous, shallow-water conglomerates and arenites. By contrast, in the eastern Almopias (also known as Meglenitsa Unit) Sharp and Robertson (1994) have described an ophiolite sequence including a volcanic section with MORB affinity covered by black schists, Callovian - Upper Jurassic radiolarites (Stais et al., 1990) and Upper Jurassic - Lower Cretaceous deep-sea turbidites. Ophiolites of the Almopias sub-Zone are interpreted as derived from a former oceanic basin (Almopias Ocean of Brown and Robertson, 2004) that subducted eastwards underneath the Serbo-Macedonian Massif. During the Late Jurassic, ophiolites from this ocean were obducted westwards onto the Pelagonian zone (Mercier et al., 1975; Bébien et al., 1994; Sharp and Robertson, 1994; Brown and Robertson, 2004). Recently, Saccani et al. (2008) concluded that the Almopias ophiolites have formed in an intra-oceanic island arc setting, as suggested by the widespread occurrence of supra-subduction zone-type (SSZ) ophiolites, such as IAT, boninites and harzburgites.

In the Paikon sub-Zone (Mercier, 1966; Mercier et al., 1975; Brown and Robertson, 2004) two main different tectonic units, the Pre-Peonian and the Paikon Units, respectively cropping out in the east and in the west, have been distinguished. The Paikon Unit consists of a Triassic to Upper Jurassic succession where metasediments interfingering with metalavas are preserved (Sharp and Robertson, 1994). The protoliths of the metalavas are represented by rhyolites, andesites and basalts of Jurassic age, according to the paleontological findings in the metasedimentary intercalations found in the metalavas. This sequence of the Paikon sub-Zone is affected by several deformation phases characterized by low-grade blueschist facies. The geochemistry of the magmatic rocks from Paikon Unit indicate that they have originated in an arc setting developed during the Middle to Late Jurassic times in consequence of an east-dipping oceanic subduction (Mercier, 1966; Vergély and Mercier, 2000; Brown and Robertson, 2004). The Triassic to Upper Jurassic sequence is unconformably topped by Upper Jurassic to Lower Cretaceous limestone topped by Upper Cretaceous turbidites, both unaffected by high-pressure metamorphism.

The Peonias sub-Zone is represented only by the Guevgueli Unit, which consists of an Upper Jurassic ophiolite sequence intruded by the granitoid intrusive complex of the Fanos Granite (Sariç et al., 2008). This unit, unaffected by metamorphism, can be subdivided in two different sub-units, reported as West and East Guevgueli sub-Units (Fig. 2). To the east, the Guevgueli Unit is thrust by the westernmost units of Serbo-Macedonian Massif, corresponding to the Pre-Rhodopian Zone. The Guevgueli ophiolitic Complex is considered to have formed in an ensialic back-arc basin opening to the east of the Paikon arc during Middle to Late Jurassic (Bébien, 1982; Bébien et al., 1987; Brown and Robertson, 2004).

Geology of the Guevgueli Unit

In the study area, the Guevgueli Unit is sandwiched between the Serbo-Macedonian Massif in the east and the Paikon Unit in the west (Fig. 1b). The boundaries of the Guevgueli Unit are represented in both east and west side by a north-south striking thrust zone. The field relationships of the studied magmatic rocks have been investigated in both West and East Guevgueli sub-units. According to Bébien (1977; 1982; 1983) and Bébien et al. (1986; 1987), both the sub-units consist of an ophiolite sequence represented only by a crustal section, without remnants of mantle rocks, probably detached during the tectonics related to emplacement onto the continental margin.

The West Guevgueli sub-Unit (Fig. 2) consists of an intrusive complex characterized by both layered and isotropic levels, in turn topped by a volcano-sedimentary complex that includes basaltic sills, pillow-lavas, pillow-breccias and hyaloclastites. The layered level of the intrusive complex includes both ultramafic (plagioclase wehrlite, clinopyroxenite, and pyroxenite) and mafic (gabbro) rocks, showing a

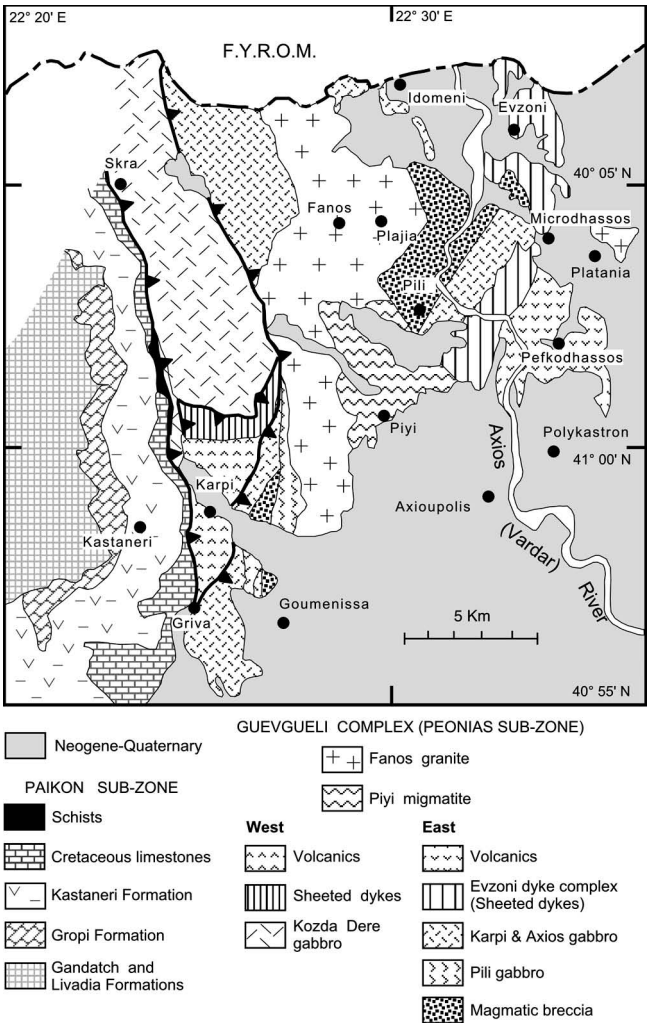

Fig. 2 - Simplified geological map of the Guevgueli Complex. Modified from Bébien and Gagny (1979) and Pe-Piper and Piper (2002).

well developed compositional layering striking N-S with regular easternward low-angle dipping. The isotropic level includes gabbros showing both fine- and coarse-grained types. The upper part of the isotropic level is represented by Fe-gabbros and Fe-diorites cut by dykelets of plagiogranites. Dm-thick shear zones characterized by gabbro-derived mylonites are also identified in both the layered and isotropic level. All the levels of the intrusive complex are cut by dm-thick dykes of gabbros (also very coarse grained) and basalts. The intrusive complex is topped by a sill complex (Mavro Dendro sills of Bébien, 1983) represented by coarse-grained basalts. The field evidence suggests that the present-day boundary between the intrusive and the sill complexes is represented by a shear zone, probably corresponding to a thrust. At the top of the sill complex a thick volcano-sedimentary sequence consisting of pillow-lava basalts alternating with levels of pillow-lava breccias and hyaloclastites occurs. Swarm of basaltic dykes have been found in the volcano-sedimentary complex. In the West Guevgueli sub-Unit no remnants of the sedimentary cover has been preserved.

The East Guevgueli sub-Unit (Fig. 2) includes an intrusive complex, similar to that of the West sub-Unit, topped by a well-developed sheeted dyke complex showing a transition to a volcano-sedimentary complex. The intrusive complex is characterized in its lower part by a well developed layering showing N-S strike with dip ranging from sub-horizontal to high angle. The intrusive complex is topped by a sheeted dyke complex, showing a great range of lithotypes from basalts to dacites, each characterized by different texture and grain-size, from fine to coarse. The strike of the dykes in the sheeted dyke complex is N-S with high-angle dipping toward both east and west. The transition from intrusive to sheeted dyke complex is characterized by the occurrence of Fe-gabbros and Fe-diorites cut by dykelets of plagiogranites. At the top of the intrusive complex, magmatic breccias consisting of gabbro fragments set in a plagiogranite matrix can be recognized (Pili magmatic breccia of Bébien, 1982). Likewise in the western subunits, the volcano-sedimentary complex includes a sill complex topped by pillow lava basalts alternating with levels of pillow breccias and hyaloclastites. In the Axios Valley (Fig. 2), where the volcanic section is well exposed, a thick sequence of basalts, andesites, dacites and rhyolites cut by basaltic dykes crops out. Differently from the West sub-Unit, the East Guevgueli is characterized by a sedimentary cover represented by Oxfordian radiolarian cherts (Danelian et al., 1996).

The age of the Guevgueli ophiolite sequence is constrained by radiometric datings by Spray et al., (1984) (149±3 and 163±3 Ma by K-Ar on mineral separates of gabbros) and Zachariadis et al. (2006) (169±1 Ma by U-Pb ion microprobe (SHRIMP II) from zircon separates of plagiogranites). In addition, an age of 164 Ma has been provided by single-zircon U-Pb method for the rhyolites at the top of the volcano-sedimentary complex from eastern Guevgueli sub-Unit (Anders et al., 2005). These data fit very well with the Oxfordian age deduced from the radiolarian assemblage in the sedimentary cover (Danelian et al., 1996).

The Guevgueli ophiolite sequence is intruded by the Fanos Granite, which consists of granitoids of Late Jurassic age (Borsi et al., 1966; Mercier, 1966; Bébien, 1982; Christofides et al., 1990; Anders et al., 2005). This granite is interpreted to have derived from lower crustal melts that differentiated mainly through fractional crystallization processes (Sariç et al., 2008). Dykes of granitoids cutting all the levels of the ophiolite sequence are recognized in the field in both the West and East Guevgueli sub-Units. The granitoids are in turn cut by a swarm of mafic dykes. An intrusive contact between granitoids and ophiolites can be observed in the East sub-Unit, whereas the boundary between the granitoids and the West sub-Unit is represented by a shear zone (Fig. 2). The age of the granitoids range from 150±2 Ma (Borsi et al., 1966) to 158 Ma (Anders et al., 2005).

The granitic rocks show primary relationships with a continental basement complex, known as the Piyi Complex (Fig. 2), which consists of orthogneisses, micaschists and amphibolites. Datings by single-zircon U-Pb method by Anders et al. (2005) suggest a Carboniferous age of the basement, regarded as derived from Serbo-Macedonian Massif by Zachariadou and Dimitriadis (1995).

SAMPLING AND ANALYTICAL METHODS

A total of 84 samples were collected from the Guevgueli Complex for petrographic and chemical analysis. Sampling was mainly focused on mafic rocks of both intrusive and ex-

trusive facies. The Fanos Granite and Piyi migmatite (Fig. 2) were not sampled. Samples taken from the West Guevgueli ophiolites mainly include gabbroic rocks and associated dykes, as well as few ultramafic cumulates from the Kozda Dere gabbro, pillow lava basalts and associated dykes from the West Guevgueli volcanic sequence. Samples from the East Guevgueli ophiolites include gabbroic rocks and crosscutting dykes from the Karpi, Axios, and Pili gabbros (Fig. 2), a few samples from the Magmatic Breccia Formation, and various subvolcanic and volcanic rocks from the Sheeted Dyke (Evzoni Dike Complex) and Volcanic sequence. Volcanic rocks include mafic, intermediate, and acidic varieties in both pillow and massive lava flows.

Samples were analyzed for major and trace elements (Zn, Ni, Co, Cr, V, Rb, Sr, Ba, Th, Nb, La, Ce, Pb, Zr, Y) by X-ray fluorescence (XRF) on pressed-powder pellets using an automated ARL Advant-X spectrometer with the matrix correction method proposed by Lachance and Trail (1966). Accuracy and detection limits were determined using international standards run as unknown. Accuracy is better than 2% for major oxides, whereas, accuracy and detection limits for trace element are better than 10% and 1-2 ppm, respectively. Volatiles were determined as loss on ignition at 1000°C.

Thirty three representative samples were chosen for additional trace element analyses, including the rare earth elements (REE), Sc, Nb, Hf, Ta, Th, and U, using a VG Elemental Plasma Quad PQ2 Plus inductively coupled plasma-mass spectrometer (ICP-MS). The accuracy and detection limits were calculated using results for international standard rocks with certified values and the blind standards included in the sample set. Accuracy is in the range of 0.9-7.9%, with the exception of Gd (10.2%). Detection limits are (in ppm): Sc = 0.2; Y = 0.1; Nb, Hf, Ta = 0.02; REE < 0.10; Th, U = 0.009. All analyses were performed at the Department of Earth Sciences of the University of Ferrara. Results are presented in Table 1.

PETROGRAPHY

Most of the samples have experienced low-grade ocean floor metamorphism under static conditions, which variably modified the primary mineralogical phases, but did not change the primary igneous textures. Nonetheless, the prefix meta- will be omitted for simplicity. As will be illustrated in the next chapter, three different groups of samples, sometimes showing common primary textures, occur in the Guevgueli Complex; thus their petrographic description is given here in the context of these three groups (Table 1).

Ultramafic plutonic and gabbroic rocks

The ultramafic rocks include serpentinized lherzolite and olivine clinopyroxenite from the Karpi Gabbro Formation, as well as plagioclase wehrlite and pyroxenite from the Kozda Dere Unit (Fig. 2). These ultramafic rocks are strongly serpentinized and bear few relic minerals other than spinel, namely olivine and clinopyroxene. The original texture is discernible by the bastite and mesh structure of serpentine minerals. The textural observation indicates a cumulitic nature with olivine as the cumulus phase and plagioclase and clinopyroxene as intercumulus minerals. Most spinel grains occur as tiny, equant, discrete crystals.

The gabbroic rocks of both West and East Guevgueli (Fig. 2) include olivine gabbro, gabbro, and amphibole diorite and their fine-grained varieties. Gabbro is dominant in all formations, whereas olivine gabbro and diorite are scarce and very scarce, respectively. Gabbroic rocks with abundant iron minerals (Ferrogabbro) are present only in the Kozda Dere Formation. The grain size in gabbroic rocks is generally 1 or 2 mm. Fine-grained varieties are common in gabbro dykes and in diorite, while pegmatitic rocks are very rare. About 90% of West Guevgueli gabbroic rocks show cumulitic textures, while almost equal abundances of cumulitic and isotropic textures are observed in intrusive rocks from East Guevgueli. Cumulitic varieties are characterized by the occurrence of clinopyroxene poikilitically including olivine and plagioclase crystals. Isotropic gabbros have idiomorphic plagioclase and sub-idiomorphic clinopyroxene. Diorite displays idiomorphic plagioclase, sub-idiomorphic clinopyroxene and amphibole, anhedral quartz, and skeletal opaque minerals. In all rock types, alteration products consist of prhenite and calcite over plagioclase, chlorite and serpentine replacing olivine, chlorite and tremolite-actinolite over clinopyroxene and amphibole. Several samples are also affected by quartz and/or calcite veins. Textural evidences suggest an olivine-plagioclase-clinopyroxene crystallization sequence, which is characteristic of MORB magmatism. Inverted pigeonite locally occurs around olivine crystals in olivine gabbro, also indicating a tholeiitic magma series.

Group 1 volcanic and subvolcanic rocks

These rocks include pillow and massive lava flows from the volcanic series of both East and West Guevgueli, as well as a number of dykes in the Magmatic Breccia, Axios Gabbro, Karpi Gabbro, and Kozda Dere Formations (Fig. 2). All these rocks are aphyric or sparsely porphyric with less than 5% microphenocrysts of plagioclase. An intersertal, fine-grained groundmass with tiny microlites of plagioclase, clinopyroxene and opaque minerals is generally observed. Coarse-grained, doleritic texture is locally observed in some massive lavas. In these rocks, alteration is generally strong and resulted in the replacement of primary minerals with prhenite, calcite, and chlorite. Veins and amygdales filled by quartz and calcite are rather common.

Group 2 volcanic and sub-volcanic rocks

This rock variety mainly occurs as massive lava flows and sheeted-dykes in the Evzoni Dyke Complex of East Guevgueli. Individual dykes are also found in the Magmatic Breccia, Axios Gabbro, Kozda Dere gabbro Formations and both East and West volcanic series (Fig. 2). In addition, basaltic pillows (e.g., sample EP107) are found in the East volcanic series. These rocks range from basalt to basaltic andesite, andesite, dacite, and rhyolite. They are mainly porphyritic with phenocryst assemblages including olivine, plagioclase and clinopyroxene in basalts, either clinopyroxene or clinopyroxene and plagioclase in basaltic andesite and andesite, plagioclase and quartz in dacite and rhyolite. Groundmass is commonly hyalophitic to intersertal and rarely intergranular. Dacite and rhyolite rarely display micro-spherulitic crystalline groundmass. Aphyric texture is locally observed in basalts and dacites. These rocks show a devitrified groundmass. The major alteration products are epidote, calcite, chlorite, tremolite-actinolite amphibole, and opaque minerals. Veins filled by quartz and zeolite are common in all rock types.

Table 1 - Bulk-rock major and trace element analyses of selected samples from the Guevgueli Complex.

	Plutonic rocks													
Sub-unit	East	East	West	West	East	East	East	East	East	East	East	East	East	West
Formation	KG	KG	KDG	KDG	MB	MB	KG	KG	KG	AG	AG	AG	AG	KDG
Locality	Karpi	Griva	Skra	Skra	Mcd	Mcd	Karpi	Karpi	Griva	Mcd	Mcd	Pfd	Pfd	Skra
Sample	EP113	GG49	GG46	EP95	GG13	GG12	EP115	EP118	GG50	GG8	GG9	GG29	GG30	GG38
Rock	Pl-Wr Pod in Gb	Ol-Cpx.te Pod in Gb	Pl-Wr	Px.te	Ol-Gb	Gb	Gb	Gb Dy in MLF	Gb	Gb	Gb	Gb	Di	Ol-Gb
Texture	cumulitic	cumulitic	cumulitic	cumulitic	cumulitic	cumulitic	isotropic	isotropic	isotropic	isotropic	isotropic	cumulitic	isotropic	isotropic
XRF Analyses:														
SiO_2	37.24	47.80	38.24	38.59	43.92	49.48	46.75	46.89	50.08	45.74	45.12	46.30	60.02	46.37
TiO_2	0.04	0.16	0.13	0.12	0.37	0.73	0.09	0.13	0.84	0.23	0.20	0.26	1.17	0.19
Al_2O_3	5.27	5.36	5.85	4.55	9.05	17.71	16.78	16.97	18.56	20.04	18.66	16.49	14.37	20.24
Fe_2O_3					1.19	0.92	0.39	0.54	0.65	0.66	0.63	0.68	1.22	0.67
FeO	5.97	11.44	8.02	14.91	7.94	6.13	2.61	3.62	4.34	4.37	4.17	4.52	8.13	4.47
MnO	0.13	0.10	0.13	0.18	0.14	0.12	0.11	0.14	0.08	0.10	0.09	0.10	0.12	0.10
MgO	39.67	23.76	34.82	32.45	26.60	8.58	14.31	13.13	7.66	10.59	12.70	13.13	2.44	9.65
CaO	0.08	4.24	3.23	2.42	7.21	11.92	12.65	12.89	12.77	15.03	14.59	15.35	5.60	15.91
Na_2O	0.05	n.d.	n.d.	0.02	0.74	2.07	2.24	0.53	2.58	1.16	0.99	0.80	5.11	1.17
K_2O	0.01	0.03	0.01	0.01	0.32	0.46	0.02	0.98	0.12	0.07	0.07	0.03	0.03	0.01
P_2O_5	n.d.	0.08	0.05	n.d.	0.23	0.46	n.d.	n.d.	0.62	0.48	0.48	0.53	0.42	0.55
L.O.I.	11.64	6.84	9.54	6.77	2.33	1.38	4.02	4.18	1.67	1.52	2.30	1.79	1.29	0.66
Total	100.10	99.81	100.02	100.03	100.04	99.96	99.97	100.02	99.96	99.98	99.99	99.98	99.90	100.00
Mg#	92.2	80.8	89.8	79.5	85.7	71.4	90.7	86.6	75.9	81.2	84.4	83.8	34.9	79.4
Zn	48	62	48	92	65	46	15	34	20	26	24	28	34	25
Ni	1498	964	1224	250	898	123	342	303	80	146	211	163	6	137
Co	95	139	104	116	94	31	29	36	28	29	37	36	16	34
Cr	3675	4068	1831	42	1339	395	1499	1265	107	565	923	481	7	421
V	38	93	53	65	128	210	85	111	99	124	115	137	34	107
Rb	n.d.	7	n.d.	n.d.	13	18	n.d.	25	3	3	4	2	n.d.	n.d.
Ba	9	26	24	3	40	127	29	175	124	57	61	41	27	44
Th	n.d.	n.d.	n.d.	n.d.	4	n.d.	n.d.	n.d.	n.d.	n.d.	n.d.	n.d.	2	n.d.
Nb	1	n.d.	n.d.	1	1	2	n.d.	1	2	n.d.	n.d.	n.d.	7	2
La	n.d.	n.d.	n.d.	n.d.	n.d.	16	n.d.	n.d.	6	2	6	n.d.	9	n.d.
Ce	4	11	n.d.	17	17	13	2	2	17	14	11	2	21	13
Pb	n.d.	n.d.	n.d.	4	10	5	2	4	3	n.d.	n.d.	4	4	7
Sr	11	12	11	16	117	274	155	44	332	223	209	120	212	98
Zr	5	5	6	2	37	89	4	7	83	5	4	8	311	10
Y	3	4	4	4	9	16	4	6	25	8	7	8	75	8
ICP-MS Analyses:														
Sc							29.3	30.8	26.6			37.3		
La							0.51	0.57	5.14			0.52		
Ce							1.04	1.19	15.6			1.81		
Pr							0.15	0.17	2.53			0.31		
Nd							0.76	0.91	13.1			1.73		
Sm							0.35	0.43	3.89			0.72		
Eu							0.18	0.26	1.13			0.33		
Gd							0.41	0.60	4.08			0.85		
Tb							0.07	0.10	0.74			0.16		
Dy							0.49	0.69	4.56			1.15		
Ho							0.10	0.14	0.97			0.26		
Er							0.28	0.41	2.59			0.71		
Tm							0.04	0.06	0.37			0.11		
Yb							0.28	0.37	2.44			0.66		
Lu							0.04	0.05	0.35			0.09		
Nb							0.43	0.61	1.84			0.60		
Hf							0.11	0.15	1.80			0.27		
Ta							0.20	0.21	0.27			0.31		
Th							0.16	0.49	0.45			0.04		
U							0.07	0.07	0.10			n.d.		
Ti/V														
Zr/Y	1.8	1.2	1.7	0.5	4.3	5.5	0.9	1.1	3.3	0.7	0.5	1.0	4.2	1.3
Nb/Y	0.39			0.13	0.13	0.12	0.11	0.1	0.07			0.08	0.09	0.27
Ce/Y	1.2	2.89		3.99	2.01	0.83	0.3	0.19	0.63	1.7	1.51	0.23	0.28	1.67
$(La/Sm)_N$							0.99	0.85	0.85			0.46		
$(Sm/Yb)_N$							1.33	1.11	1.77			1.21		
$(La/Yb)_N$							1.31	0.95	1.51			0.56		
$(Tb/Yb)_N$							1.14	1.23	1.38			1.10		

Abbreviations, BABB- backarc basin basalt; CAB- calc-alkaline; KG- Karpi Gabbro; KDG- Kozda Dere Gabbro; MB- Magmatic Breccia; AG- Axios Gabbro; EVS- East Volcanic Series; EDC- Evzoni Dyke Complex; WVS- West Volcanic Series; Mcd- Microdhassos; Pfd- Pefkodhassos; Plt- Platania; Pl-Wr- plagioclase wehrlite; Ol-Cpx.te- Olivine clinopyroxenite; Px.te- Pyroxenite; Ol-Gb- olivine gabbro; Gb- gabbro; Di- diorite; B- basalt; BA- basaltic andesite; A- andesite; D- dacite; R- rhyolite; Dy- dyke; MLF- massive lava flow; Sh-Dy- sheeted dyke; n.d.- not detected. Fe2O3 = 0.15 FeO; Mg# = molar Mg/(Mg+Fe)*100.

Table 1 (*continued*)

	Plutonic rocks						Group 1 (BABB) volcanic and subvolcanic rocks							
Sub-unit	West	West	West	West	West	West	East	East	East	East	East	East	East	East
Formation	KDG	KDG	KDG	KDG	KDG	KDG	MB	AG	AG	KG	KG	KG	EVS	EVS
Locality	Skra	Skra	Skra	Skra	Skra	Skra	Axios R.	Pfd	Pfd	Karpi	Karpi	Karpi	Pfd	Axios R
Sample	GG41	EP93	GG44	EP94	EP100	GG47	GG15	GG28	GG26	GG56	GG55	GG54	GG24	GG33
Rock	Ol-Gb	Gb	Gb	Gb	Gb	Gb	B	B	B	B	BA	B	B	BA
Type							Dy in Granite	Dy in Di	MLF	Dy in Gb	Dy in Gb	Dy in Pillow	Pillow	MLF
Texture	cumulitic	cumulitic	cumulitic	cumulitic	cumulitic	cumulitic	aphiric	aphiric	doleritic	aphiric	aphiric	aphiric	aphiric	aphiric
XRF Analyses:														
SiO_2	48.63	48.32	42.03	46.63	43.62	45.56	46.77	47.48	48.89	51.97	55.70	52.53	44.63	54.17
TiO_2	0.59	0.41	2.63	0.68	2.53	1.75	0.67	1.06	1.09	1.70	1.61	1.13	1.20	1.45
Al_2O_3	18.64	18.81	14.75	16.62	15.49	16.07	14.40	15.87	16.59	15.82	15.49	15.28	16.99	15.68
Fe_2O_3	0.80	0.93	1.96	1.04	1.78	1.37	1.12	1.25	1.23	1.53	1.37	1.40	1.03	1.15
FeO	5.35	6.22	13.09	6.96	11.84	9.15	7.45	8.35	8.18	10.21	9.13	9.32	6.86	7.64
MnO	0.12	0.14	0.15	0.15	0.16	0.15	0.15	0.15	0.15	0.14	0.13	0.19	0.17	0.12
MgO	8.32	10.47	9.53	11.34	9.90	8.48	13.51	9.18	8.42	5.55	4.29	7.10	10.14	4.17
CaO	14.25	12.42	12.81	13.37	12.39	13.75	12.28	10.32	8.61	6.53	8.73	9.17	6.80	4.40
Na_2O	2.38	2.17	1.64	1.52	1.69	2.22	1.13	2.99	3.63	5.03	2.84	1.88	3.47	6.66
K_2O	0.02	0.02	0.02	0.02	0.01	0.03	0.14	0.44	0.63	0.03	0.03	0.04	1.65	0.22
P_2O_5	0.46	n.d.	0.38	n.d.	n.d.	0.40	0.43	0.37	0.30	0.22	0.32	0.31	0.83	0.20
L.O.I.	0.41	0.06	1.03	1.62	0.54	1.03	1.95	2.54	2.26	1.26	0.35	1.55	6.20	4.16
Total	99.96	99.98	100.03	99.95	99.96	99.96	99.99	100.01	99.98	99.99	99.98	99.90	99.98	100.01
Mg#	73.5	75.0	56.5	74.4	59.8	62.3	76.4	66.2	64.7	49.2	45.6	57.6	72.5	49.3
Zn	24	37	66	35	73	56	55	31	36	51	26	26	57	86
Ni	39	77	137	43	47	56	304	60	61	9	7	31	103	11
Co	27	44	60	43	62	46	47	41	38	30	27	24	27	22
Cr	136	384	50	288	90	196	912	140	158	23	20	81	403	25
V	200	195	1350	274	925	532	236	264	259	436	353	306	182	291
Rb	2	n.d.	2	n.d.	n.d.	2	8	16	25	n.d.	3	n.d.	48	9
Ba	39	14	13	15	9	44	44	70	70	35	29	30	253	52
Th	n.d.	n.d.	n.d.	n.d.	n.d.	n.d.	n.d.	n.d.	n.d.	n.d.	n.d.	n.d.	n.d.	4
Nb	n.d.	n.d.	2	n.d.	n.d.	n.d.	2	2	n.d.	2	1	2	2	6
La	n.d.	2	n.d.	n.d.	4	n.d.	4	4	7	6	8	7	8	10
Ce	8	13	15	1	19	2	8	10	6	15	26	12	14	25
Pb	3	n.d.	7	n.d.	5	n.d.	9	4	n.d.	2	4	3	6	6
Sr	182	140	107	141	149	164	112	173	204	139	201	159	119	55
Zr	10	9	12	9	10	12	40	96	93	121	166	75	90	193
Y	7	12	11	11	13	10	17	24	24	32	40	24	25	45
ICP-MS Analyses:														
Sc				44.8		50.3	32.4	38.4		37.2		32.0		
La				0.30		0.49	2.21	3.32		6.55		4.93		
Ce				1.15		1.80	6.05	9.82		16.6		13.1		
Pr				0.24		0.33	0.93	1.56		2.42		1.99		
Nd				1.51		2.10	4.48	7.62		12.0		9.50		
Sm				0.78		1.04	1.52	2.54		3.87		2.83		
Eu				0.45		0.55	0.52	0.92		1.27		1.01		
Gd				1.02		1.51	1.73	3.08		4.36		3.35		
Tb				0.18		0.26	0.32	0.54		0.80		0.59		
Dy				1.30		1.84	2.13	3.52		5.12		3.78		
Ho				0.29		0.42	0.46	0.75		1.08		0.88		
Er				0.80		1.19	1.35	2.19		3.16		2.43		
Tm				0.12		0.18	0.20	0.32		0.47		0.37		
Yb				0.72		0.99	1.36	2.14		3.00		2.34		
Lu				0.11		0.14	0.21	0.30		0.42		0.36		
Nb				0.28		0.40	1.65	2.07		2.41		1.86		
Hf				0.30		0.46	1.16	1.78		2.81		1.89		
Ta				0.21		0.22	0.35	0.33		0.38		0.26		
Th				n.d.		0.02	0.58	0.32		0.81		0.51		
U				n.d.		n.d.	0.21	0.12		0.23		0.14		
Ti/V							17	25	26	24	27	22	42	31
Zr/Y	1.4	0.8	1.1	0.9	0.8	1.3	2.4	4	3.9	3.8	4.2	3.2	3.6	4.3
Nb/Y			0.18	0.03		0.04	0.1	0.09		0.08	0.03	0.08	0.09	0.13
Ce/Y	1.08	1.1	1.31	0.11	1.5	0.18	0.36	0.41	0.26	0.52	0.65	0.55	0.54	0.56
$(La/Sm)_N$				0.25		0.31	0.94	0.84		1.09		1.12		
$(Sm/Yb)_N$				1.20		1.16	1.24	1.32		1.43		1.35		
$(La/Yb)_N$				0.30		0.35	1.17	1.11		1.57		1.51		
$(Tb/Yb)_N$				1.14		1.19	1.07	1.15		1.21		1.15		

Table 1 (*continued*)

	Group 1 (BABB) volcanic and subvolcanic rocks												Group 2 (CAB)	
Sub-unit	East	East	West	West	West	West	West	West	West	West	West	West	East	East
Formation	EVS	EVS	KDG	KDG	KDG	KDG	WVS	WVS	WVS	WVS	WVS	WVS	MB	MB
Locality	Axios R.	Pfd	Skra	Skra	Skra	Skra	Karpi	Karpi	Karpi	Griva	Karpi	Karpi	Axios R.	Axios R.
Sample	GG34	GG31	GG39	EP96	EP97	EP98	GG57	GG58	EP110	GG52	EP109	GG59	GG11	GG16
Rock	B	D	B	B	B	B	B	B	B	B	BA	A	B	B
Type	MLF	MLF	Dy in Gb	Dy in Gb	Dy in Gb	Dy in Gb	MLF	MLF	MLF	Pillow	MLF	MLF	Dy in MB	Dy in MB
Texture	aphiric	aphiric	aphiric	aphiric	aphiric	aphiric	aphiric	aphiric	aphiric	porphiric	aphiric	aphiric	aphiric	doleritic
XRF Analyses:														
SiO_2	47.50	59.82	49.59	48.68	49.11	49.60	51.05	44.63	50.82	51.67	55.37	57.92	51.87	52.41
TiO_2	1.75	1.22	1.21	0.80	0.84	1.90	1.57	1.52	0.82	1.78	1.21	1.56	1.09	0.77
Al_2O_3	15.88	12.64	16.53	15.50	16.26	16.15	13.75	14.75	17.87	16.47	16.29	15.09	17.29	19.62
Fe_2O_3	1.53	1.18	1.40	1.24	1.21	1.64	1.63	1.31	1.28	1.56	1.21	1.19	1.14	0.88
FeO	10.18	7.88	9.36	8.25	8.06	10.94	10.86	8.74	8.54	10.42	8.07	7.94	7.61	5.86
MnO	0.26	0.13	0.15	0.16	0.16	0.17	0.15	0.19	0.18	0.24	0.18	0.15	0.14	0.12
MgO	7.73	2.73	7.90	10.44	9.30	8.16	6.99	8.24	8.60	6.37	7.00	4.53	5.98	4.75
CaO	5.19	4.58	9.49	10.46	11.14	9.05	10.29	10.66	3.50	6.76	1.68	3.41	9.97	9.48
Na_2O	4.96	5.20	2.96	2.22	2.32	0.81	1.00	3.48	3.99	3.75	5.42	5.91	3.16	3.45
K_2O	0.05	0.37	0.08	0.03	0.03	0.01	0.02	0.27	0.98	0.08	0.03	0.27	0.47	0.75
P_2O_5	0.21	0.36	0.44	0.06	0.06	0.12	0.34	0.37	0.09	0.48	0.40	0.22	0.41	0.35
L.O.I.	4.80	3.79	0.88	2.07	1.44	1.48	2.37	5.82	3.27	0.38	3.11	1.81	0.86	1.32
Total	100.03	99.92	99.98	99.91	99.94	100.03	100.02	100.00	99.95	99.96	99.97	100.01	99.99	99.75
Mg#	57.5	38.2	60.1	69.3	67.3	57.1	53.4	62.7	64.2	52.2	60.7	50.4	58.4	59.1
Zn	339	109	29	44	44	18	92	90	144	88	153	140	57	43
Ni	15	11	46	47	48	12	13	42	47	12	3	5	35	28
Co	29	14	47	46	45	31	39	40	36	35	13	12	32	23
Cr	39	6	85	57	49	29	26	83	50	21	6	2	56	44
V	362	53	302	249	245	432	450	340	301	399	51	89	284	210
Rb	n.d.	10	n.d.	n.d.	n.d.	n.d.	n.d.	4	13	2	2	n.d.	19	30
Ba	26	53	32	14	15	14	26	50	181	29	19	49	282	288
Th	n.d.	n.d.	n.d.	n.d.	n.d.	2	3	n.d.	1	n.d.	2	6	2	4
Nb	6	9	2	1	2	2	2	3	2	n.d.	5	8	2	3
La	9	11	4	5	5	8	n.d.	4	6	n.d.	15	9	8	9
Ce	22	28	13	12	12	17	22	14	15	19	38	46	20	28
Pb	10	7	2	3	7	6	4	4	8	9	6	8	6	7
Sr	57	56	185	199	199	454	222	231	199	61	42	109	462	414
Zr	182	306	89	60	64	112	76	135	52	114	273	319	114	110
Y	40	68	24	25	26	40	27	33	24	39	90	64	21	20
ICP-MS Analyses:														
Sc	35.6	22.7	38.8	34.5	30.3	27.1		33.7	31.1		15.4		25.7	21.0
La	8.32	10.1	3.50	4.16	4.25	7.26		6.21	5.23		14.4		7.15	10.6
Ce	20.5	27.6	10.6	10.5	10.6	19.4		15.1	12.6		39.9		17.2	24.5
Pr	2.96	4.58	1.69	1.58	1.63	2.93		2.21	1.77		5.93		2.36	3.27
Nd	13.8	24.3	8.60	8.19	8.42	13.9		11.3	8.83		30.3		9.83	14.1
Sm	4.20	7.46	2.89	2.58	2.65	4.37		3.58	2.66		9.89		2.67	3.51
Eu	1.39	2.54	1.00	0.92	0.98	1.30		1.17	0.96		2.90		0.91	1.24
Gd	4.53	8.89	3.05	2.89	3.18	4.84		3.39	2.94		11.1		2.92	3.73
Tb	0.83	1.66	0.54	0.53	0.53	0.88		0.75	0.50		2.18		0.47	0.57
Dy	5.21	10.3	3.54	3.42	3.47	5.69		4.97	3.19		13.7		3.06	3.5
Ho	1.08	2.24	0.73	0.78	0.73	1.27		1.13	0.71		3.05		0.63	0.74
Er	3.09	6.20	2.14	2.11	2.11	3.48		3.03	1.90		7.46		1.78	2.16
Tm	0.44	0.92	0.32	0.32	0.31	0.51		0.46	0.31		1.09		0.25	0.33
Yb	2.85	5.65	2.05	2.03	2.04	3.25		2.94	1.94		7.22		1.73	2.19
Lu	0.41	0.83	0.31	0.33	0.30	0.46		0.44	0.29		0.97		0.25	0.34
Nb	6.01	7.42	1.53	1.83	1.85	1.93		3.92	1.82		4.94		2.14	3.51
Hf	3.23	6.13	1.91	1.81	1.89	2.42		3.12	1.67		7.13		1.80	1.92
Ta	0.44	0.62	0.23	0.22	0.22	0.37		0.42	0.17		0.39		0.30	0.25
Th	0.64	0.89	0.34	0.34	0.36	0.99		0.40	0.87		1.58		2.59	3.56
U	0.26	0.73	0.06	0.12	0.09	0.21		0.22	0.20		0.57		1.43	1.41
Ti/V	30	144	24	20	21	24	21	29	17	25	147	107	23	22
Zr/Y	4.6	4.5	3.7	2.4	2.4	2.8	2.9	4.1	2.2	2.9	3.0	5.0	5.4	5.6
Nb/Y	0.15	0.11	0.06	0.07	0.01	0.05	0.09	0.12	0.08		0.05	0.12	0.1	0.18
Ce/Y	0.51	0.4	0.44	0.42	0.4	0.48	0.82	0.46	0.52	0.48	0.44	0.72	0.8	1.25
$(La/Sm)_N$	1.28	0.87	0.78	1.04	1.04	1.07		1.12	1.27		0.94		1.73	1.95
$(Sm/Yb)_N$	1.64	1.47	1.57	1.41	1.44	1.49		1.35	1.52		1.52		1.72	1.78
$(La/Yb)_N$	2.09	1.28	1.23	1.47	1.49	1.60		1.51	1.94		1.43		2.97	3.47
$(Tb/Yb)_N$	1.32	1.34	1.20	1.19	1.18	1.23		1.16	1.17		1.37		1.23	1.18

Table 1 (*continued*)

	Group 2 (CAB) volcanic and subvolcanic rocks													
Sub-unit	East	East	East	East	East	East	East	East	East	East	East	East	East	West
Formation	MB	MB	AG	EVS	EVS	EDC	EDC	EDC	EDC	EDC	EDC	EDC	EDC	WVS
Locality	Axios R.	Axios R.	Mcd	Plt	Pfd	Mcd	Mcd	Mcd	Mcd	Axios R.	Evzoni	Evzoni	Evzoni	Karpi
Sample	GG17	GG14	GG6	EP107	GG32	GG3	GG4	GG5	GG2	GG35	GG20	GG21	GG22	EP111
Rock	B	B	B	B	D	B	B	B	BA	BA	A	D	R	D
Type	Dy in MB	Dy in Granite	Dy in Gb	Pillow	Dy in GG31	Sh-Dy	Sh-Dy	Sh-Dy	Sh-Dy	Dy	MLF	MLF	MLF	Dy in MLF
Texture	aphiric	aphiric	aphiric	aphiric	porphiric	porphiric	porphiric	porphiric	porphiric	aphiric	porphiric	aphiric	porphiric	porphiric
XRF Analyses:														
SiO_2	49.55	50.31	48.65	48.06	65.99	50.86	50.33	48.33	52.93	53.58	56.10	59.40	71.18	67.53
TiO_2	1.04	0.69	0.78	0.77	0.80	0.73	0.83	0.68	1.06	0.94	0.58	1.13	0.35	0.65
Al_2O_3	17.39	16.24	16.02	13.32	14.95	16.22	16.72	16.02	16.72	15.51	11.88	13.72	13.53	15.37
Fe_2O_3	0.92	1.07	1.10	0.77	0.62	0.98	1.10	1.05	1.22	1.33	0.98	1.41	0.32	0.40
FeO	6.11	7.15	7.36	5.11	4.15	6.53	7.30	7.00	8.13	8.86	6.51	9.41	2.14	2.70
MnO	0.11	0.13	0.14	0.17	0.06	0.13	0.13	0.13	0.14	0.13	0.12	0.12	0.03	0.12
MgO	6.58	9.43	10.94	7.30	2.68	10.16	7.73	13.54	6.46	6.27	4.85	6.06	1.40	2.30
CaO	8.70	10.56	8.39	9.26	1.03	6.97	9.22	7.79	7.64	5.10	10.88	1.60	1.05	1.33
Na_2O	2.55	2.08	3.25	1.77	4.32	3.63	2.34	1.41	2.66	5.03	6.36	4.45	3.98	7.85
K_2O	2.59	0.38	0.26	0.82	3.76	0.98	1.01	0.69	0.82	0.44	0.03	0.04	3.95	0.11
P_2O_5	0.44	0.38	0.31	0.06	0.05	0.24	0.35	0.28	0.33	0.18	0.83	0.18	0.05	0.19
L.O.I.	3.99	1.48	2.78	12.57	1.55	2.45	3.04	3.10	1.87	2.62	0.85	2.46	1.91	1.46
Total	99.97	99.89	99.98	99.98	99.96	99.90	100.10	100.03	99.97	99.98	99.98	99.99	99.90	100.01
Mg#	65.7	70.2	72.6	71.8	53.5	73.5	65.4	77.5	58.6	55.8	57.0	53.4	53.9	60.3
Zn	53	36	53	43	46	68	41	65	81	93	50	93	33	72
Ni	42	170	121	171	7	147	56	238	25	10	233	8	9	4
Co	25	35	37	27	10	35	33	38	31	26	40	14	6	4
Cr	65	362	326	542	4	264	133	521	56	21	588	10	19	7
V	216	251	226	163	81	237	249	228	298	361	159	68	46	26
Rb	75	19	10	11	110	28	36	27	27	11	n.d.	2	93	2
Ba	1088	223	126	181	633	273	260	229	375	251	267	131	723	34
Th	16	3	2	2	6	4	4	3	6	9	6	3	11	1
Nb	10	2	n.d.	5	6	1	2	2	3	3	1	10	3	2
La	53	5	4	9	11	11	10	8	12	12	28	13	13	8
Ce	108	14	11	24	25	23	20	17	29	25	58	40	37	31
Pb	18	5	4	7	n.d.	4	8	3	8	6	11	4	3	6
Sr	700	452	300	272	111	309	307	209	411	284	366	29	43	105
Zr	201	78	79	67	164	96	92	91	132	121	93	353	140	137
Y	26	16	19	16	27	18	23	17	23	20	13	73	19	43
ICP-MS Analyses:														
Sc	24.4	30.8	26.3	25.2	7.40		23.3	26.6	21.5	35.5	22.2			
La	54.2	7.70	5.09	9.39	10.7		7.51	6.53	12.4	14.2	26.4			
Ce	109	18.2	12.5	21.1	24.6		17.2	15.3	27.9	29.7	54.6			
Pr	12.4	2.58	1.73	2.46	3.28		2.4	2.17	3.75	3.86	7.21			
Nd	41.9	11.5	7.61	10.0	12.6		11.0	9.92	16.6	16.2	25.9			
Sm	7.21	2.99	2.07	2.40	3.07		3.04	2.6	3.93	3.77	5.56			
Eu	1.84	1.03	0.73	0.72	0.72		1.07	0.92	1.35	1.19	1.34			
Gd	5.24	3.09	2.54	2.03	2.90		3.5	2.92	4.19	4.06	3.55			
Tb	0.64	0.48	0.43	0.33	0.45		0.58	0.47	0.63	0.59	0.47			
Dy	3.63	2.83	2.77	2.07	2.75		3.6	2.84	3.74	3.46	2.36			
Ho	0.65	0.60	0.58	0.40	0.56		0.8	0.61	0.78	0.72	0.42			
Er	1.91	1.69	1.69	1.06	1.67		2.24	1.73	2.22	1.99	1.15			
Tm	0.24	0.25	0.26	0.16	0.25		0.34	0.26	0.33	0.29	0.16			
Yb	1.73	1.63	1.64	1.08	1.76		2.23	1.68	2.14	1.83	1.00			
Lu	0.25	0.25	0.24	0.16	0.26		0.34	0.27	0.34	0.28	0.15			
Nb	8.81	2.03	0.97	4.26	6.06		2.43	2.03	3.69	3.31	2.04			
Hf	5.00	1.96	1.89	1.48	6.23		2.41	2.16	3.05	2.84	2.01			
Ta	1.08	0.26	0.27	0.30	0.63		0.22	0.23	0.27	0.23	0.62			
Th	13.3	2.41	1.51	2.08	4.68		3.51	3.32	4.98	8.07	7.60			
U	2.97	0.92	0.47	0.85	2.72		1.21	1.19	1.79	2.64	0.91			
Ti/V	30	17	21	27	60	19	21	19	22	16	20	103	47	151
Zr/Y	7.7	4.8	4.1	4.2	6.0	5.4	4.0	5.4	5.7	6.1	7.4	4.8	7.3	3.2
Nb/Y	0.34	0.13	0.05	0.27	0.22	0.07	0.11	0.12	0.16	0.17	0.16	0.13	0.17	0.05
Ce/Y	4.2	1.12	0.64	1.33	0.91	1.32	0.75	0.9	1.22	1.49	4.31	0.55	1.95	0.74
$(La/Sm)_N$	4.85	1.66	1.59	2.53	2.25		1.60	1.62	2.04	2.43	3.06			
$(Sm/Yb)_N$	4.63	2.04	1.40	2.47	1.93		1.51	1.72	2.05	2.29	6.16			
$(La/Yb)_N$	22.46	3.39	2.23	6.25	4.34		2.41	2.78	4.17	5.58	18.86			
$(Tb/Yb)_N$	1.68	1.34	1.19	1.39	1.16		1.18	1.27	1.34	1.47	2.14			

GEOCHEMISTRY

Elements, which are virtually immobile during low-temperature alteration and metamorphism (Beccaluva et al., 1979; Pearce and Norry, 1979; Shervais, 1982) will be used for describing the major and trace element geochemistry of the samples studied in this paper. Generally, immobile elements include incompatible elements, such as Ti, P, Zr, Y, Sc, Nb, Ta, Hf, Th, middle (M-) and heavy (H-) REE, as well as some transition metals (e.g., Ni, Co, Cr, V). Large ion lithophile elements (LILE) are commonly mobilized during alteration, whereas light REE (LREE) may be affected by some mobilization during alteration. However, the good correlations between LREE and many immobile elements (not shown) indicate that these elements have been only slightly mobilized by the alteration. Similarly, the good correlation existing between Ba, SiO_2, Al_2O_3, FeO, MgO and other relatively immobile elements (e.g., r^2 Ba vs. Zr = 0.70; r^2 SiO_2 vs. Zr = 0.77; r^2 FeO vs. Zr = 0.60) suggests that these elements were not significantly affected by mobilization during alteration and can therefore reasonably be used.

Ultramafic plutonic and gabbroic rocks

The plutonic rocks are represented by plagioclase wehrlite, olivine clinopyroxenite and pyroxenite with Mg# ranging from 79.0 to 92.4. No substantial chemical differences are observed between rocks belonging to the East and West ophiolites. The Al_2O_3 and CaO contents in these rocks are rather variable but generally low, 1.59-8.13 wt% and 0.06-4.68 wt%, respectively. The TiO_2 content varies from 0.01 to 0.54 wt%. They are very depleted in Rb, Zr, Y, and Th (Table 1). High concentrations of Ni, Co, and Cr are consistent with the olivine and spinels accumulation observed through the petrographic analyses.

The gabbros analyzed include both cumulitic and isotropic varieties. Significant chemical differences are observed between the two textural types. Cumulitic gabbros show higher values of TiO_2 (0.26-2.63 wt%), total FeO (4.92-14.85 wt%), MgO (7.66-26.60 wt%), Zr (8-89 ppm), and Y (7-25 ppm) with respect to isotropic gabbros (TiO_2: 0.09-0.23 wt%; total FeO: 2.96-5.07 wt%; MgO: 9.65-14.31 wt%; Zr: 4-10 ppm; Y: 4-8 ppm). Compatible elements (Ni, Co, Cr, V) are generally more abundant in cumulitic rocks than in isotropic types (Table 1). Only a very primitive

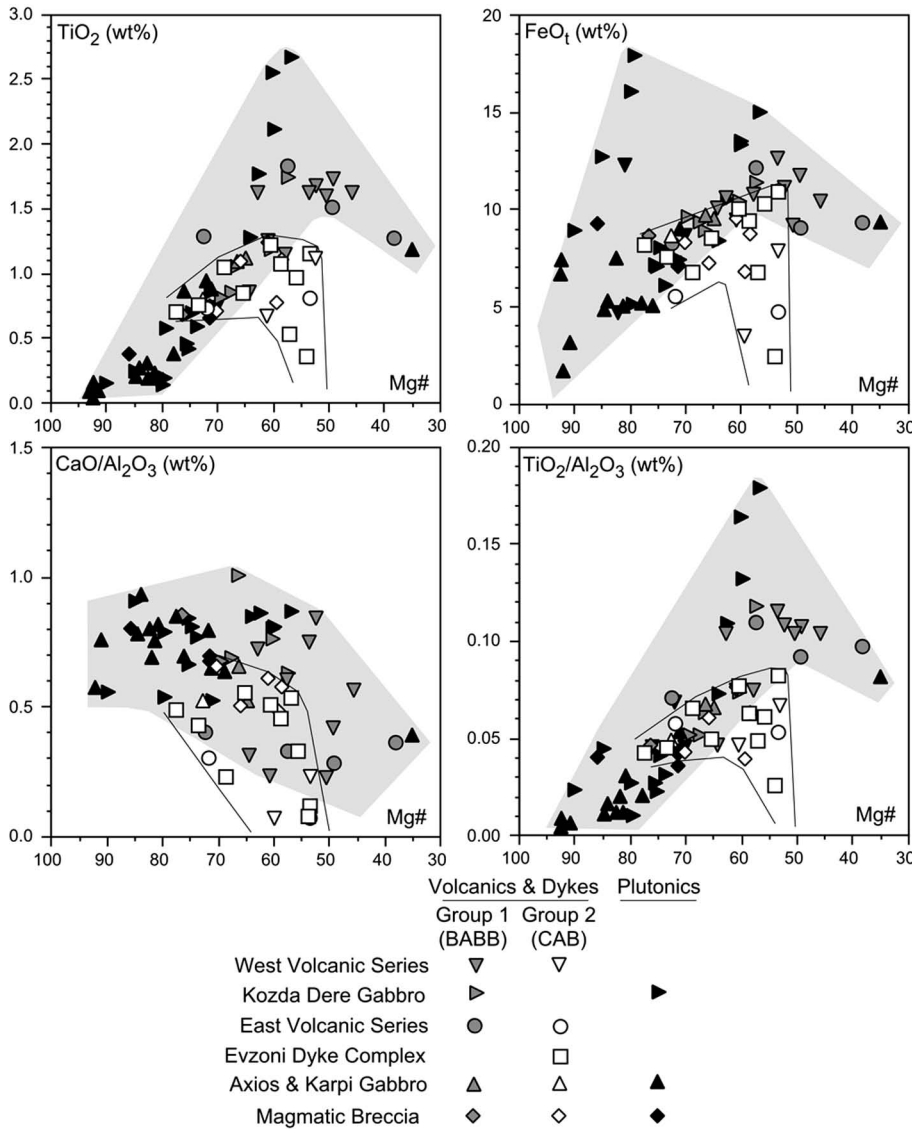

Fig. 3 - Selected element and elemental ratio vs. Mg# variation diagrams for Jurassic plutonic, subvolcanic, and volcanic rocks from the Guevgueli Complex. Grey fields and lines encompass the chemical variation of Group 1 (BABB) and Group 2 (CAB) rocks, respectively. Abbreviations, BABB- back-arc basin basalt; CAB- calc-alkaline basalt.

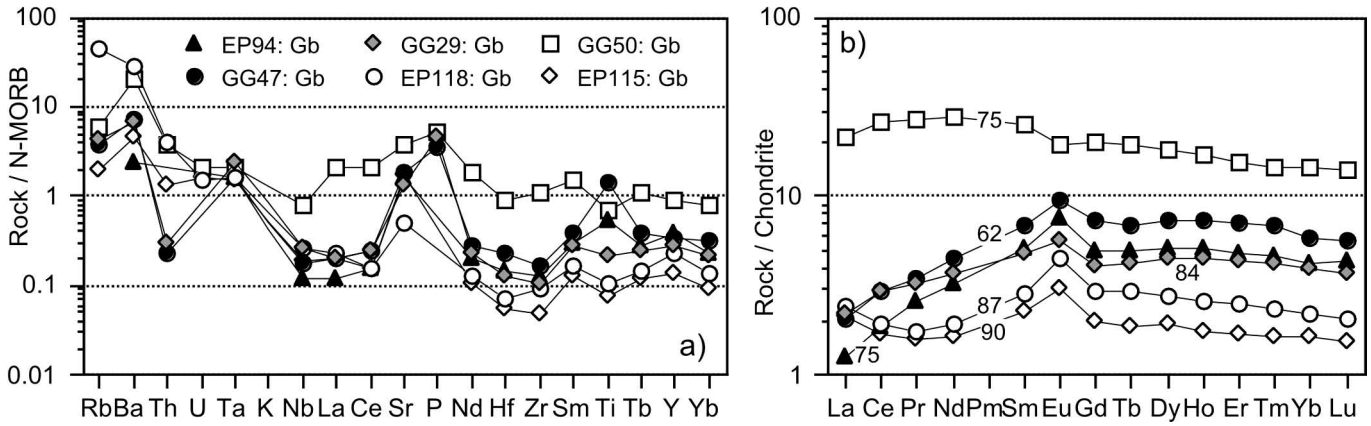

Fig. 4 - N-MORB normalized incompatible element patterns (a) and chondrite-normalized REE patterns (b) for gabbroic rocks from the Guevgueli ophiolites. Normalizing values are from Sun and McDonough (1989). Abbreviations as in Table 1. Solid and grey-filled symbols: cumulitic rocks; open symbols: isotropic rocks. Figures in Fig. 4b indicate the Mg# values.

isotropic gabbro (EP115) shows high content of Cr (1499 ppm). In the variation diagrams of Fig. 3 cumulitic gabbros from the Kozda Dere Formation show strong TiO_2, FeO_t, and TiO_2/Al_2O_3 increasing with decreasing Mg#, chosen as differentiation index.

The high field strength element (HFSE) and REE concentrations (Fig. 4) are generally correlated with the Mg# values. Both cumulitic and isotropic varieties display positive Eu anomalies (Fig. 4b), with the exception of sample GG50, which represents a rather differentiated rock. This is consistent with the early fractionation and cumulus of plagioclase observed through the petrographic analyses. Cumulitic gabbros are characterized by depletion of LREE with respect to HREE. By contrast, primitive isotropic gabbros EP115 and EP118 show a marked La and Ce enrichment with respect other LREE (Fig. 4b). The more evolved isotropic gabbro GG50 is characterized by LREE/HREE enrichment.

There is no chemical distinction between the coarse- and fine-grained gabbros. The gabbro dykes that cut the gabbros or lava flows (e.g., EP118, Table 1) have compositions indistinguishable from the other gabbros and are different from the lavas, which indicates that they do not probably represent a late stage of the axial sequence. In the discrimination diagram of Fig. 5, all gabbroic rocks plot in the field for high-Ti ophiolitic gabbros. In summary, ultramafic plutonic and gabbroic rocks have overall geochemical characteristics that resemble those of similar rocks generated in a mid-ocean ridge setting.

Group 1 volcanic and subvolcanic rocks

Group 1 volcanic and subvolcanic rocks generally range from basalt to basaltic andesite (SiO_2: 44.63-55.70 wt%), while more evolved rocks, such as andesite and dacite (Table 1), are very scarce. Basalt and basaltic andesite are relatively rich in TiO_2 (0.80-1.88 wt%), Al_2O_3 (13.75-17.51 wt%), Zr (52-182 ppm), and Y (24-90 ppm). Nonetheless, Zr contents in the less evolved basalts (40-70 ppm) are somewhat lower than in typical primitive MORB (72-73 ppm; Sun and McDonough, 1989). They are also relatively rich in Ni (9-103 ppm) and Cr (21-403 ppm).

In the variation diagrams of Fig. 3, Group 1 rocks display marked enrichment of TiO_2, FeO_t and TiO_2/Al_2O_3 with decreasing Mg# from the most primitive to the moderately evolved rocks, followed by a decrease towards the more evolved rocks. This feature is typical of high-Ti tholeiitic series from mid-ocean ridge and back-arc. HFSE (e.g., Nb, Ta, Hf, Sm, Zr and Y) classically show a steady increase with decreasing Mg# (not shown in this paper). The CaO/Al_2O_3 ratio regularly decreases with diminishing Mg#; however, this decrease is much less pronounced that in Group 2 rocks (Fig. 3). This is consistent with early crystallization of plagioclase with respect to clinopyroxene, as already observed through the petrographic analyses.

The normal-type MORB (N-MORB) normalized incompatible element and the chondrite-normalized REE patterns of these rocks are shown in Fig. 6. Rocks from East (Fig. 6a, b) and West (Fig. 6c, d) Guevgueli show very similar compositions and are both characterized by incompatible element patterns steadily decreasing from LILE (e.g., Rb, Ba, U, Th) to HFSE (e.g., Ta, Nb, Hf, Zr, Sm, Ti, Y, Yb), as well as by flat, or slightly LREE-enriched patterns, with La_N/Yb_N ranging from 1.11 to 2.09.

On the Th/Yb vs. Ta/Yb diagram (Fig. 7), these rocks show elemental ratios, which may resemble those of E-MORB (Sun and McDonough, 1989). Nonetheless, many

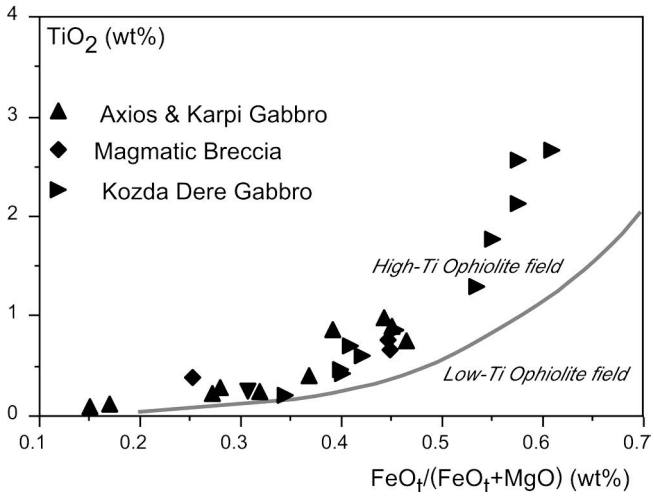

Fig. 5 - TiO_2 vs. FeO_t/FeO_t + MgO discrimination diagram for gabbroic rocks from the Guevgueli Complex ophiolites. Modified from Serri (1981).

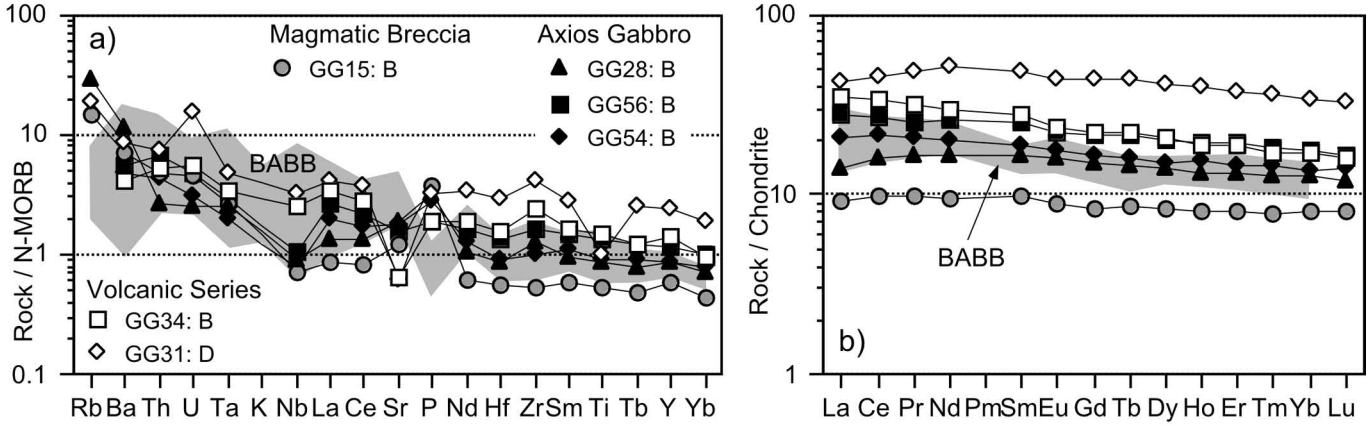

Fig. 6 - N-MORB normalized incompatible element patterns (a, c) and chondrite-normalized REE patterns (b, d) for Group 1 volcanic and subvolcanic rocks from the Guevgueli ophiolites. Normalizing values are from Sun and McDonough (1989). Compositional variations (grey fields) of back-arc basin basalts (BABB) from the New Hebrides back-arc basin (Maillet et al., 1995) are reported for comparison. Abbreviations as in Table 1.

basaltic lavas from the West Volcanic series and basaltic dykes from the Kozda Dere gabbros (West Guevgueli) are influenced by a subduction component, having relatively high Th/Yb ratios coupled with relatively low Ta/Yb ratios. In contrast, this subduction component is less pronounced, or even absent, in the basaltic lavas and dykes from the East Guevgueli Units. In summary, Group 1 volcanic and subvolcanic rocks show geochemical characteristics very similar to those observed in back-arc basin basalts (BABB) as, for example, in BABB from the New Hebrides back-arc (Maillet et al., 1995).

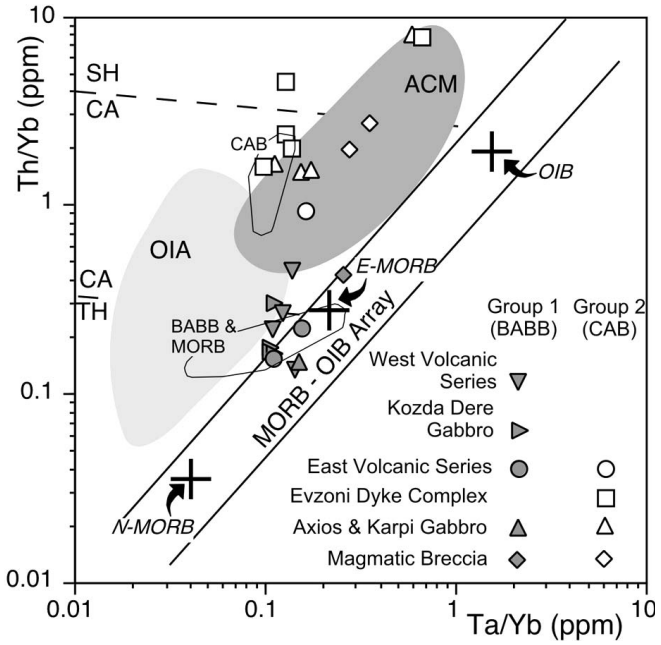

Fig. 7 - Th/Yb vs. Ta/Yb diagram (modified from Pearce, 1982) for the Jurassic volcanic and subvolcanic rocks from the Guevgueli Complex. Compositions of modern N-MORB, E-MORB and OIB (crosses) are from Sun and McDonough (1989). Open fields indicate the compositional variations of modern calc-alkaline (CAB), back-arc basin (BABB), and mid-ocean ridge (MORB) basalts from the New Hebrides back-arc basin (Maillet et al., 1995). Grey fields represent the compositional variations of oceanic island arc (OIA) and active continental margin (ACM) basalts from various modern and ancient tectonic settings (Pearce, 1983).

Group 2 volcanic and sub-volcanic rocks

Group 2 volcanic and subvolcanic rocks range in composition from basalt to basaltic andesite, andesite, dacite and rhyolite (Table 1), where basalts and basaltic andesites are largely prevailing in volume. Basaltic rocks are relatively poor in TiO_2 (0.53-1.21 wt%), Zr (40-201 ppm), and Y (13-26 ppm) but relatively rich in Al_2O_3 (13.32-19.62 wt%), when compared to Group 1 rocks. Cr, Ni, and V contents are highly variable (Table 1) and are strictly positively correlated with the variation of the Mg# (not shown), suggesting that their variation is closely controlled by the fractionation processes. Andesites, dacites and rhyolites contain low amounts of TiO_2 (0.18-1.13 wt%), Ni (4-9 ppm), Cr (2-19 ppm), and V (2-81) and relatively high amounts of Zr (137-353 ppm), and Y (19-73 ppm).

In the variation diagrams of Fig. 3, Group 2 rocks display a little, or even absent, enrichment of TiO_2, FeO_t and TiO_2/Al_2O_3 with decreasing Mg# from basalts to basaltic andesites, followed by a sharp decrease towards the more evolved rocks. This feature is typical of sub-alkaline series from orogenic tectonic settings. HFSE show a marked increase with decreasing Mg# (not shown in this paper). The CaO/Al_2O_3 ratios (Fig. 3) sharply decrease with diminishing Mg#; this is consistent with the early crystallization of

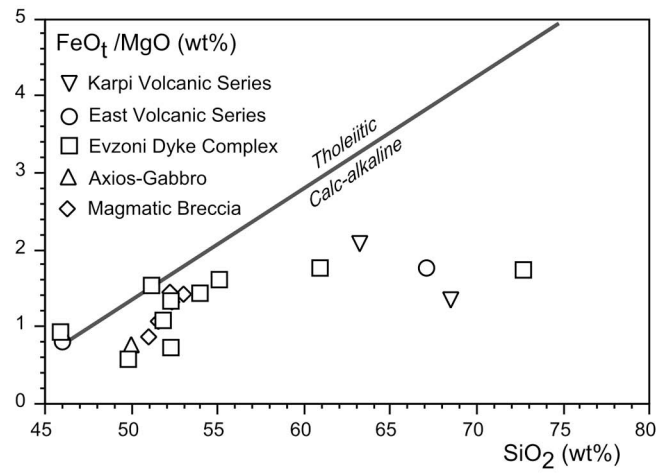

Fig 8 - SiO2 vs. FeO_t/MgO diagram (modified from Miyashiro, 1974) for the Group 2 volcanic and subvolcanic rocks from the Guevgueli Complex.

clinopyroxene with respect to plagioclase, as observed by the petrographic analyses.

FeO_t/MgO ratios plotted against SiO_2 (Fig. 8) suggest a calc-alkaline affinity for Group 2 volcanic and subvolcanic rocks. Incompatible and REE patterns (Fig. 9) are consistent with these conclusions. Actually, as commonly observed in calc-alkaline rocks from volcanic arc settings, Group 2 rocks are generally characterized by LILE (Rb, Ba, Th, U) enrichment and HFSE (Ti, Tb, Y, Yb) depletion, relative to N-MORB, with positive anomalies of K, La, Ce and marked negative anomalies of Ta, Nb, Hf, and Ti (Figs. 9a, c). REE display strong LREE/HREE enriched patterns (Fig. 9b, d), with La_N/Yb_N ratios ranging from 1.2 to 22.5.

Group 2 volcanic and subvolcanic rocks show high Th/Yb ratios with respect to Ta/Yb ratios (Fig. 7), suggesting that these rocks are clearly influenced by an arc geochemical component (Pearce, 1982). High Ba/Zr ratios (between 1 and 5) are also commonly considered as an indicator of the extent of arc signature (Fryer et al., 1990). In fact, Ba/Zr ratios observed in Group 2 volcanic and subvolcanic rocks (1.5-5.4) are typical of volcanics from island-arc environments. In summary, based on their overall geochemical characteristics, Group 2 volcanic and subvolcanic rocks can be classified as a calc-alkaline (CAB) series generated at destructive plate margin.

DISCUSSION

Petrogenesis and tectono-magmatic implications

One of the most striking traits of the Guevgueli Complex is the contemporaneous occurrence of magmatic rocks with different geochemical signatures, namely, MORB-like intrusive rocks, MORB-like extrusive rocks with BABB characteristics, and both intrusive and extrusive calc-alkaline rocks. It is, therefore, important to reveal if any petrogenetic relationships among these rocks exists in order to understand the magmatic processes taking place in the Guevgueli oceanic basin, which may have significant implications for the geodynamic processes controlling the evolution of the Vardar Ocean.

For this purpose, we examined the behaviour of some incompatible elements (mostly, HFSE), and especially their inter-element relationships (Th/Yb, Th/Ta, Th/Tb, Ba/Zr and Nb/Zr). These elements generally have low bulk distribution coefficient (D) in basic magmas. Amphibole that occurs in some of the more evolved products has a relatively high D for these elements. Petrographic evidence suggests, however, that the amount of amphibole separation is too small to seriously affect the behaviour of these elements in rocks ranging from basalts to dacites. It can therefore be assumed that these elements behave as incompatible irrespective of whether fractional crystallization or partial melting is involved, but their inter-element relationships do not change drastically during such processes and are representative of the composition of the source material.

Moreover, the nature (degree of depletion) and degree of melting of the mantle source(s) can be inferred by plotting a compatible versus an incompatible element, since compatible element abundance is not significantly modified during the progressive mantle source depletion, whereas abundance of incompatible elements is closely related to source deple-

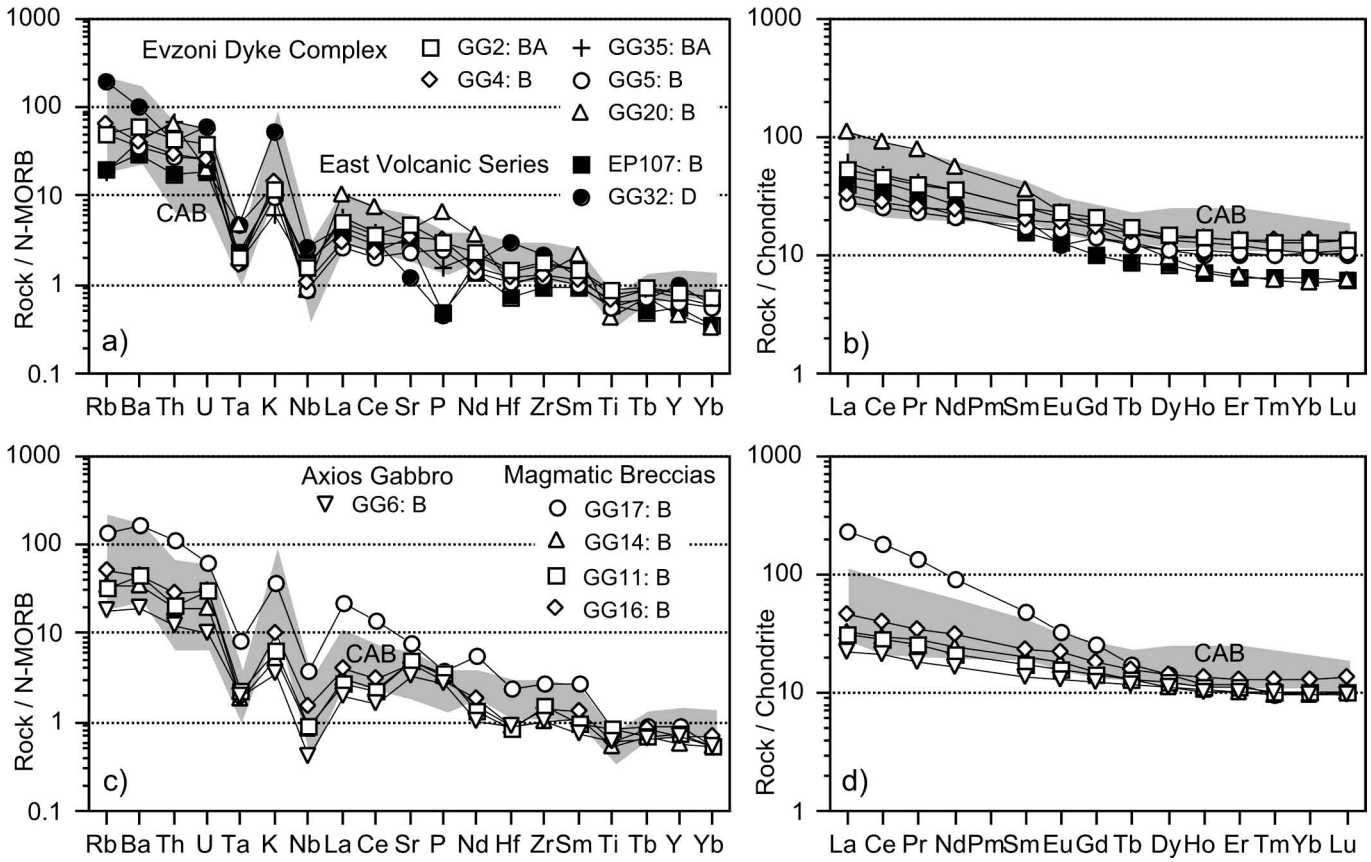

Fig. 9 - N-MORB normalized incompatible element patterns (a, c) and chondrite-normalized REE patterns (b, d) for Group 2 (calc-alkaline) volcanic and subvolcanic rocks from the Guevgueli Complex. Normalizing values are from Sun and McDonough (1989). Compositional variations (grey fields) of calc-alkaline volcanic rocks from the New Hebrides back-arc basin (Maillet et al., 1995) are reported for comparison. Abbreviations as in Table 1.

tion and degree of melting (Pearce, 1982; 1983). For this purpose, the Cr vs. Y diagram of Fig. 10 illustrates an attempt to depict the possible mantle sources and relative degrees of partial melting of the different lava types studied in this paper.

The Group 2 calc-alkaline volcanic and subvolcanic rocks are compatible with about 15-20% partial melting from a depleted mantle source (Fig. 10). All these rocks have Th/Yb ratios greater than unit (Fig. 7) and many of them are HREE-depleted (Fig. 9b, d). The HREE-depleted patterns observed in CAB samples form the Guevgueli Complex are consistent with melting of garnet peridotite (McKenzie and O'Nions, 1991). This suggests that the magma producing these CAB rocks was derived from deep levels within the mantle. Nonetheless, some CAB rocks do not display significant HREE fractionation with respect to medium REE. This implies that these rocks may have derived from relatively shallow levels within the mantle. The chondrite-normalized patterns crossing each other (Fig. 9b, d) actually indicate that CAB rocks have derived from slightly different mantle sources. Calc-alkaline rocks are considered reliable petrogenetic indicators of subduction-related processes (Pearce, 1982). These typically show lower abundances of HFSE and higher abundances of LILE, relative to N-MORB with depletions in Nb, Ta, and Ti. These chemical features observed in CAB rocks from the Guevgueli Complex are thus interpreted as imprints of subduction-related processes. Bébien (1982) has demonstrated that during the Middle to Late Jurassic times the subduction of the Almopias Oceanic branch below the Serbo-Macedonian (European) realm resulted in the formation of a volcanic arc with calc-alkaline magmatism (Paikon arc) now represented by the Paikon sub-Zone. The close association in space and time of the Guevgueli calc-alkaline rocks with the Paikon arc suggests that the Middle to Upper Jurassic calc-alkaline rocks from the Guevgueli Complex can most likely be correlated with the subduction process that originated the Paikon arc. Unfortunately, no suitable literature geochemical data are available for the Paikon arc; therefore a comparison between CAB rocks from these two units cannot be made.

Some of the Group 1 basalts and basaltic andesites are compatible with about 20% partial melting of an undepleted MORB-type source (S1). However, many of the Group 1 volcanic and subvolcanic rocks intersects the melting curve of the undepleted MORB-type source at about 40% partial melting, which is an unreasonably high degree of partial melting. Alternatively, in the model of Fig. 10 these samples intersect the melting path at about 15-20% partial melting of a depleted source (S2), calculated by Murton (1989) as the residue after 20% MORB melt extraction. From this semi-quantitative model it results that Group 1 rocks may have derived from primary melts derived, in turn, either from relatively undepleted MORB-type sources or comparatively more depleted mantle sources.

The Group 1 basalts have Nb/Zr ratio (Fig. 11), as well as Nb/Y ratio (Table 1) similar to those of N-MORB (Sun and McDonough, 1989). The Zr/Y ratios range from 2 to 4, indicating that these rocks originated from partial melting of primary mantle sources (Pearce and Norry, 1979). This suggests that, with respect to HFSE/HFSE ratios, the Guevgueli Group 1 basalts were derived from a source material analogous to that for N-MORB. However, the LILE/HFSE ratios (e.g., Th/Tb, Th/Yb, Ta/Yb, Th/Ta, and Ba/Zr) and the LREE/HREE ratios are higher than those of N-MORB. Greater concentrations of LILE in the Group 1 basalts com-

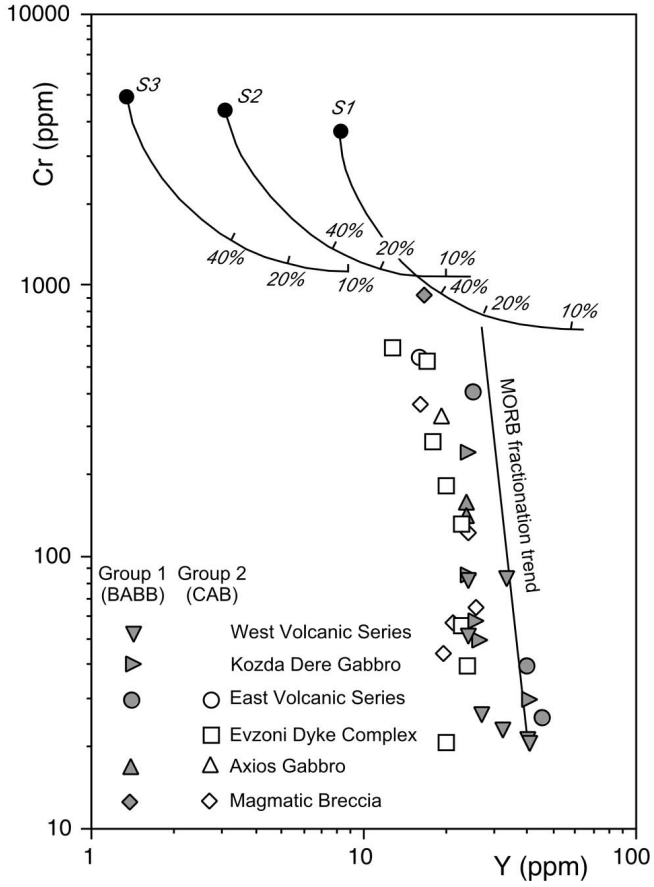

Fig. 10 - Cr vs. Y diagram for the Jurassic volcanic and subvolcanic rocks from the Guevgueli Complex. Modified after Pearce (1982). Mantle source compositions and melting paths for incremental batch melting are from Murton (1989). S1- theoretical MORB source; S2- residue after 20% MORB melt extraction from source S1; S3- residue after 12% melt extraction from source S2.

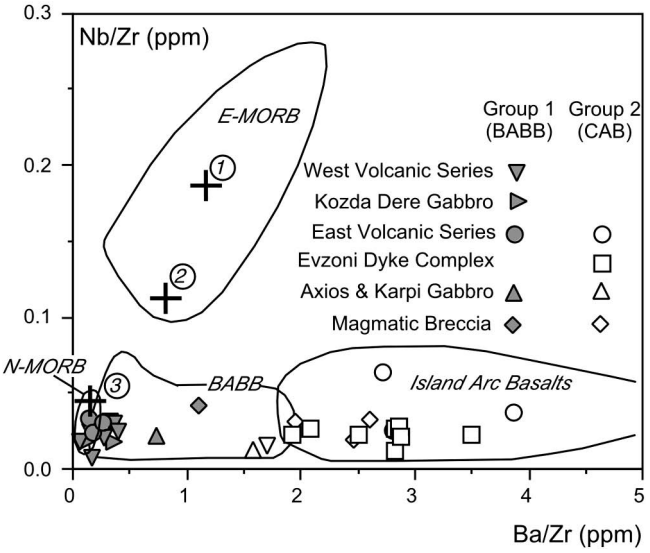

Fig. 11 - Nb/Zr vs. Ba/Zr diagram for the Jurassic volcanic and subvolcanic rocks from the Guevgueli Complex. Crosses indicate the compositions of modern OIB (1), E-MORB (2), and N- MORB (3) (Sun and McDonough, 1989). Also shown are the compositional ranges of modern normal-type (N-) and enriched-type (E-) mid-ocean ridge basalts (MORB), back-arc basin basalts (BABB), and island arc basalts from various localities (see Ishizuka et al., 1990 for data source).

pared to N-MORB cannot simply be a result of smaller degree of partial melting of N-MORB-type source material or a result of fractional crystallization, because such processes would not change the LILE/HFSE ratios with respect to the source composition. It follows that the source material of the Group 1 basalts was most likely enriched in LILE and LREE prior to melting relative to the N-MORB source material. The Th enrichment with respect to Ta is commonly used for estimating the amount of enrichment of SSZ component (Pearce, 1982). The Th/Yb ratios of many Group 1 basaltic lavas and dykes are high when compared to Ta/Yb ratios (Fig. 7) and therefore are influenced by a SSZ component. The general MORB-like chemistry coupled with an evident subduction component shown by Group 1 basalts is typical of BABB (e.g., Gribble et al., 1998).

It is widely accepted that LILE, in contrast to HFSE, are transported by aqueous fluids derived from subducted oceanic slabs and that may enrich the mantle wedge above the subducted plate. In this context, it is most likely that slab-derived components have variably modified the source material for the Guevgueli Group 1 basalts. The process responsible for such a metasomatic enrichment of the source region of Group 1 basalts is presumably related to injection of N-MORB source-like asthenosphere into the Paikon arc mantle source in consequence of the Guevgueli back-arc rifting. A similar process is also characteristic of active back-arcs such as the Scotia Sea (Saunders and Tarney, 1979), Bransfield Strait (Weaver et al., 1979), Lau and Mariana (Wood et al., 1982; Volpe et al., 1987), New Hebrides (Maillet et al., 1995).

There are no lines of evidence for generation of Group 1 basalts by mixing between MORB and CAB magma-types (e.g., xenoliths, plagioclase morphology, irregular overgrowth of clinopyroxene along margins of orthopyroxene, and reversely zoned structure of plagioclase). In addition, major and trace element data, as well as incompatible element ratios do not define a mixing trend between Guevgueli Group 1 BABB and Group 2 CAB. Likewise, there is no evidence that some E-MORB-type signatures of the Guevgueli ophiolites, e.g., LREE/HREE enrichment (Fig. 6), have derived from a primitive MORB-type source enriched by an OIB-like plume component. Actually, using diagrams (not all shown herein) where ratio vs. ratio of incompatible elements (e.g., Nb/Zr, Ce/Y, Nb/Y, Zr/Y), especially hygromagmatophile elements (e.g., Th/Tb, Th/Ta), which give an estimation of the mantle source composition (Allègre and Minster, 1978), samples from Guevgueli ophiolites are not compatible with the chemistry of a primitive MORB-type source enriched by an OIB-like component. For example, the Nb/Zr ratios of Group 1 basalts are much lower than those observed in typical E-MORBs influenced by OIB geochemical components (Fig. 11). Rather, hygromagmatophile element ratios for both BABB and calc-alkaline rocks plot along a common correlation line, suggesting that they shared similar elemental ratios in their sources. In summary, Group 1 lavas and dykes of the Guevgueli Complex have originated from partial melting of a MORB-like mantle source influenced by subduction components in a back-arc tectonic setting.

As illustrated in the previous chapters, ultramafic and gabbroic rocks from the various plutonic formations have petrographic and geochemical characteristics, which are similar to those of equivalent rocks generated at mid-ocean ridge (e.g., Fig. 5). From the variation diagrams of major elements shown in Fig. 3 it can be observed that plutonic rocks together with Group 1 volcanic and subvolcanic rocks define fractionation trends, which indicate early fractionation of olivine and plagioclase, followed by Fe-Ti oxides and clinopyroxene. This suggests co-magmatic relationships between plutonic rocks and Group 1 volcanic-subvolcanic rocks of the Guevgueli Complex. The influence of a subduction component observed in Group 1 basaltic rocks can also be observed in some gabbroic rocks. Actually, the more evolved isotropic gabbro GG50 displays LREE/HREE enrichment, whereas some primitive isotropic gabbros display La and Ce enrichment (Fig. 4b). Moreover, isotropic gabbros have relatively high Th contents and relative negative anomalies in Nb, Zr and Ti (Fig. 4b), which also suggest a derivation from partial melting of a MORB-like mantle source somewhat influenced by subduction components in a back-arc tectonic setting.

Finally, the Guevgueli Complex has been classically subdivided into two distinct sub-units (Fig. 2): the West and East Guevgueli (Bébien, 1977; 1982; Bébien and Gagny, 1979). The data presented in this paper show that both West and East sub-Units are characterized by the occurrence of both BABB and CAB rocks. Moreover, no chemical distinction can be observed within each rock type in the different sub-units; therefore a distinction in West and East Guevgueli is meaningless and should be abandoned.

Geodynamic implications

According to many authors (e.g., Şengör and Yılmaz, 1981; Robertson and Dixon, 1984; Robertson et al., 1996; Stampfli and Borel, 2002; Brown and Robertson, 2004; Bortolotti et al., 2005; Smith, 2006; Sharp and Robertson, 2006), the Vardar Zone (Fig. 1a) represents a main Tethyan suture zone, which testifies for the existence of a Mesozoic oceanic basin between the Pelagonian (to the west) and the Serbo-Macedonian (to the east) continental margins. This conclusion is based on the occurrence and geological characteristics of a number of ophiolitic complex extending (from north to south) from the Former Yugoslav Republics to the northern Greece. In particular, in the Greek sector, the Vardar Zone includes a number of ophiolitic complexes (Fig. 1a), which are basically represented by the ophiolites of the Guevgueli Complex (Peonias sub-Zone) and by the several ophiolitic complexes in the Almopias sub-Zone (Fig. 1b). These ophiolitic complexes are now separated by the Paikon sub-Zone (Fig. 1b), a tectonic window where an Upper Jurassic volcanic arc built-up onto the Serbo-Macedonian continental crust is preserved (Bébien et al., 1994; Brown and Robertson, 2004).

The Guevgueli Complex has been excellently interpreted by Bébien and co-workers (e.g., Bébien et al., 1987, and reference therein) as an ensialic backarc basin developed in a wrench zone between the Paikon volcanic arc and the continental margin of the Serbo-Macedonian Massif. The data presented in this paper confirm this hypothesis, and provide new constraints on the composition and tectono-magmatic significance of the rock associations forming the Guevgueli Complex. Actually, this backarc was characterized by the contemporaneous occurrence of BABBs and calc-alkaline lavas and dykes. The close association of coeval oceanic and continental-margin magmatic rocks can be explained as the result of the opening of the backarc basin mainly controlled by transtension (Bébien et al., 1986), leading to complex geometry of boundaries between the volcanic arc and the oceanic basin. The displacement of the continental arc

along strike-slip faults and its displacement into the oceanic basin can explain the coexistence of BABB and calc-alkaline rocks observed in the Guevgueli sub-Zone (Fig. 12). An active strike-slip tectonics can explain the on-strike changes in the chemical composition of magmas within the Guevgueli backarc. Injection of MORB-type asthenosphere into the sub-arc mantle resulted in the production of BABB-type magmas, which were erupted in the backarc area together with calc-alkaline volcanic rocks during lowermost part of the Middle Jurassic (Fig. 12).

By contrast, as shown by Saccani et al. (2008), the Almopias ophiolites, include: (1) LREE-depleted N-MORB; (2) LREE-enriched E-MORB; (3) alkaline within-plate basalts; (4) low-Ti island arc tholeiites; and (5) very-low-Ti boninites, suggesting then a composite tectonic scenario for their evolution. In fact, according to these authors, the various rock associations found in the Almopias ophiolites record several distinct accretion events in the same basin, that is: oceanic crust generation at mid-ocean ridge and alkaline seamounts in the oceanic domain; generation of SSZ ophiolites in an intra-oceanic tectonic settings located in the western (present coordinates) realm of the Serbo-Macedonian continent. A similar composite tectonic scenario is also characteristic of SSZ ophiolites in the External Ophiolite belt in Albania and Greece (e.g., Bortolotti et al., 2002; 2005; Saccani et al., 2004). Thus, ophiolites from the Almopias and Guevgueli (Peonias) sub-zones, though both belonging to the Vardar Zone, have developed in two different tectonic setting and represent two different oceanic basins separated by the Paikon volcanic arc within the Vardar Zone during the Late Jurassic times. Immediately after, probably in the Late Jurassic/Early Cretaceous time span, while the Almopias ophiolites were emplaced onto the Pelagonian continental realm, the Guevgueli ophiolites were involved at shallow structural levels in the tectonics connected with the continental collision between Adria and Eurasia Plates (e.g. Mercier, 1966; Vergély, 1984; Ricou and Godfriaux, 1991; Robertson et al., 1996; Michard et al., 1998; Pamić et al., 2002; Bortolotti et al., 2004; 2005; Saccani et al., 2004; Brown and Robertson, 2004; Smith, 2006; Sharp and Robertson, 2006).

CONCLUSIONS

The data presented in this paper indicate that the ophiolite sequence from Guevgueli Unit can be regarded as representative of a Middle-Upper Jurassic back-arc basin where two different magma types were coexisting. They include: (1) calc-alkaline magmatism represented by volcanic rocks and dykes, which can be correlated with the development of a volcanic arc onto the Serbo-Macedonian continental realm; and (2) back-arc basin magmatism, represented by the intrusive and extrusive ophiolitic sequences, which can be correlated with the injection of a MORB-type mantle source into the sub-arc mantle wedge. The coexistence of these magma-types is clearly indicated by field evidence, such as dykes of different composition crosscutting each other. The interference CAB and BABB rocks can be explained as acquired in a back-arc basin characterized by transtension, probably driven by main plates motion, where continental and oceanic areas were displaced along strike-slip faults. Moreover, the geochemistry of magmatic rocks highlight a clear difference between the Guevgueli and Almopias ophiolites that testifies for their location in two different oceanic basins. The Guevgueli ophiolites can be regarded as derived from a Middle-Upper Jurassic basin opened along the Eurasia continental margin and located between the Paikon volcanic arc and the Serbo-Macedonian Massif. By contrast, the Almopias ophiolites derived from a SSZ basin located west of the Paikon volcanic arc (Saccani et al., 2008). In summary, the possible tectono-magmatic evolution of the Guevgueli back-arc basin can be summarized as follows (Fig. 12). The subduction of the oceanic crust beneath the Serbo-Macedonian continent led to the formation of the Middle to Upper Jurassic Paikon volcanic arc onto the European continental crust. During this stage, calc-alkaline magmas were produced. Soon after, the extension in the back-arc basin, most likely associated with transtension (Bébien et al., 1986), led to the incipient formation of the Guevgueli backarc, where calc-alkaline magmas were emplaced. Meanwhile, the ongoing backarc extension was associated with the uprising of primitive asthenosphere

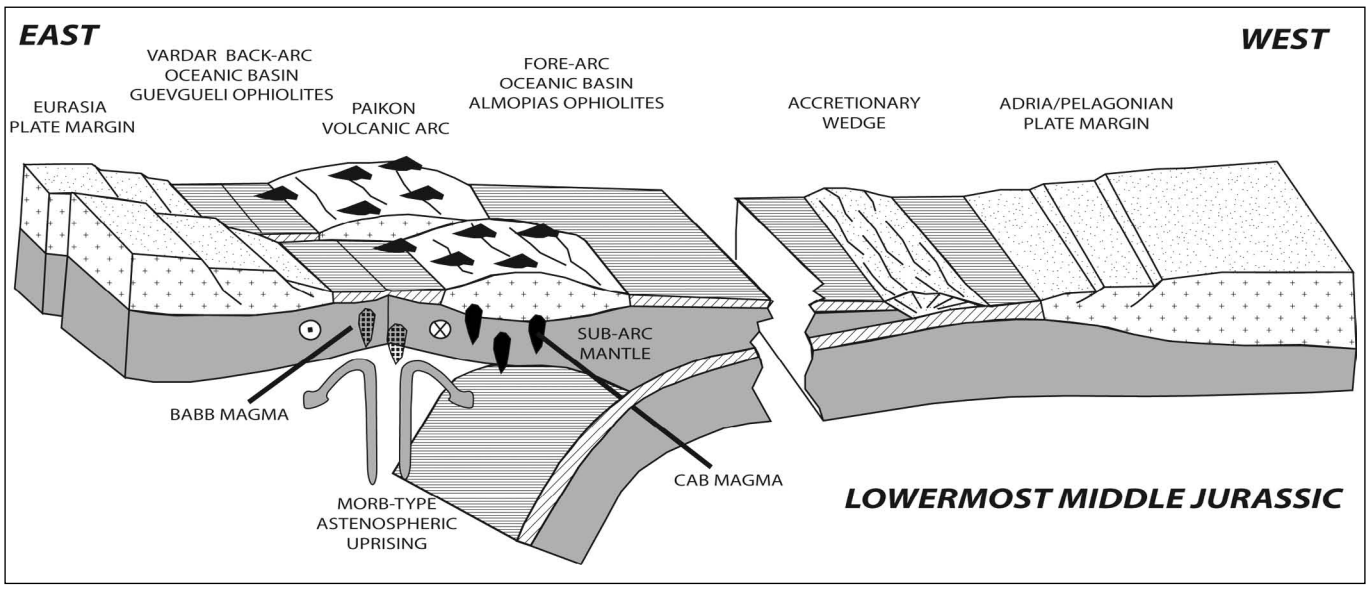

Fig. 12 - 3-D cartoon (not to scale) showing the proposed tectono-magmatic setting for the formation of back-arc basin basalts (BABB) and calc-alkaline (CAB) rocks of the Guevgueli Complex during lowermost Middle Jurassic times. A gap in the forearc region has been reported because there is no general consensus about the tectono-magmatic processes, as well as their extension, that occurred in this area during the Middle Jurassic.

and the formation of new stable spreading centre associated with generation of BABB. This history ends with the inception of tectonics related to continental collision, probably started since the Late Jurassic/Early Cretaceous times.

ACKNOWLEDGMENTS

This work was financially supported by the Italian Ministry of University (PRIN-2005 and 2006) and by the I.G.M.E. of Athens. Renzo Tassinari is thanked for assistance with XRF and ICP-MS analyses. This research was also supported by C.N.R (Istituto di Geoscienze e Georisorse) and by funds ATENEO grant by Ferrara, Firenze and Pisa Universities. M. Barth and A. Koroneos are gratefully acknowledged for their helpful reviews.

REFERENCES

Allègre C.J. and Minster J.F., 1978. Quantitative models of trace element behaviour in magmatic processes. Earth Planet. Sci. Lett., 38: 1-25.

Anders B., Reischmann T., Poller U. and Kostopoulos D., 2005. Age and origin of granitic rocks of the eastern Vardar Zone, Greece: new constraints on the evolution of the Internal Hellenides. J. Geol. Soc. London, 162: 857-870.

Bébien J., 1977. Mafic and ultramafic rocks associated with granites in the Vardar zone. Nature, 270: 232-234.

Bébien J., 1982. L'association ignée de Guevgueli (Macédonie grèque), expression d'un magmatisme ophiolitique dans une déchirure continentale. These d'Etat, Univ. Nancy, 470 pp.

Bébien J., 1983. L'association ignée de Guevgueli. Ofioliti, 8: 293-302.

Bébien J., Baroz F., Capedri S. and Venturelli G., 1987. Magmatismes basiques associés a l'ouverture d'un bassin marginal dans les Hellenides Internes au Jurassique. Ofioliti, 12: 53-70.

Bébien J., Dubois R. and Gauthier A., 1986. Example of ensialic ophiolites emplaced in a wrench zone; innermost Hellenic ophiolite belt (Greek Macedonia). Geology, 14: 1016-1019.

Bébien J. and Gagny C.I., 1979. Differenciation des magmas ophiolitiques: l'exemple du cortege de Guevgueli. In: A. Panayiotou (Ed.), Ophiolites, Proceed. Intern. Ophiolite Symp., Cyprus. Geol. Surv. Dept., Cyprus, p. 351-359.

Bébien J., Platvoet B. and Mercier, J., 1994. Geodynamic significance of the Paikon Massif in the Hellenides: contribution of the volcanic rock studies. Bull. Geol. Soc. Greece, 30: 63-67.

Beccaluva L., Coltorti M., Premti I., Saccani E., Siena F. and Zeda O., 1994. Mid-ocean ridge and suprasubduction affinities in the ophiolitic belts from Albania. Ofioliti, 19: 77-96.

Beccaluva L., Ohnenstetter D. and Ohnenstetter M., 1979. Geochemical discrimination between ocean-floor and island-arc tholeiites-application to some ophiolites. Can. J. Earth Sci., 16: 1874-1882.

Bernoulli D. and Laubscher H., 1972. The palinspastic problem of the Hellenides. Ecl. Geol. Helv., 65: 107-118.

Borsi S., Ferrara G., Mercier J. and Tongiorgi E., 1966. Age stratigraphique et radiométrique Jurassique Supérieur d'un granite des Zones Internes Hellénides (Granite de Fanos, Macédoine, Grèce). Rev. Géogr. Phys. Géol. Dyn. (2), 8: 279-287.

Bortolotti V., Carras N., Chiari M., Fazzuoli M., Marcucci M., Photiades A. and Principi G., 2003. The Argolis Peninsula in the palaeogeographic and geodynamic frame of the Hellenides. Ofioliti, 28: 79-94.

Bortolotti V., Chiari M., Kodra A., Marcucci M., Marroni M., Mustafa F., Prela M., Pandolfi L., Principi G. and Saccani E., 2006. Triassic MORB magmatism in the Southern Mirdita Zone (Albania). Ofioliti, 31: 1-9.

Bortolotti V., Chiari M., Marcucci M., Marroni M., Pandolfi L., Principi G. and Saccani E., 2004. Comparison among the Albanian and Greek ophiolites: in search of constraints for the evolution of the Mesozoic Tethys ocean. Ofioliti, 29: 1-94.

Bortolotti V., Chiari M., Marcucci M., Photiades A., Principi G. and Saccani E., 2008. New geochemical and age data on the ophiolites from the Othrys area (Greece): Implication for the Triassic evolution of the Vardar Ocean. In: A. Montanini and E. Saccani (Eds.), Geodynamic and tectono-magmatic significance of ophiolites from the peri-Mediterranean orogenic belts. Sp. Session, Ofioliti, 33: 135-152.

Bortolotti V., Kodra A., Marroni M., Mustafa F., Pandolfi L., Principi G. and Saccani E., 1996. Geology and petrology of ophiolitic sequences in the Mirdita region (Northern Albania). Ofioliti, 21: 3-20.

Bortolotti V., Marroni M., Pandolfi L. and Principi G., 2005. Mesozoic to Tertiary tectonic history of the Mirdita ophiolites, northern Albania. In: Y. Dilek, Y. Ogawa, V. Bortolotti and P. Spadea (Eds.), Evolution of ophiolites in convergent and divergent plate boundaries, The Island Arc, 14: 471-493.

Bortolotti V., Marroni M., Pandolfi L., Principi G. and Saccani E., 2002. Interaction between mid-ocean ridge and subduction magmatism in Albanian ophiolites. J. Geol., 110: 561-576.

Bortolotti V. and Principi G., 2005. Tethyan ophiolites and Pangea break-up. In: Y. Dilek, Y. Ogawa, V. Bortolotti and P. Spadea (Eds.), Evolution of ophiolites in convergent and divergent plate boundaries, The Island Arc, 14: 442-470.

Brown S.A.M. and Robertson A.H.F., 2004. Evidence of Neotethys rooted within the Vardar suture zone from the Voras Massif, northernmost Greece. Tectonophysics, 381: 143-173.

Collaku A., Cadet J.-P., Bonneau M. and Jolivet L., 1992. L'édifice structural de l'Albanie septentrionale: des éléments de réponse sur les modalités de la mise en place des ophiolites. Bull. Soc. Géol. France, 163: 455-468.

Christofides G., Soldatos T. and Koroneos A., 1990. Geochemistry and evolution of the Fanos Granite, N. Greece. Mineral. Petr., 43: 49-63.

Danelian T., Robertson A.H.F. and Dimitriadis S., 1996. Age and significance of radiolarian sediments within basic extrusives of the marginal basin Guevgueli Ophiolite (northern Greece). Geol. Mag., 133: 127-136.

Dercourt J., Ricou L.E. and Vrielynck B. (Eds.), 1993. Atlas Tethys palaeo-environmental maps. Gauthier-Villars, Paris, 307 pp.

Dilek Y., Furnes H. and Shallo M., 2007. Suprasubduction zone ophiolite formation along the periphery of Mesozoic Gondwana. Gondwana Res., 11: 453-475.

Doutsos R., Pe-Piper G., Boronkay K. and Koukouvelas I., 1993. Kinematics of the Central Hellenides. Tectonics, 12: 936-953.

Fryer P., Taylor B., Langmuir C. H. and Hochstaedter A., 1990. Petrology and geochemistry of lavas from the Sumisu and Torishima backarc rifts, Earth Planet. Sci. Lett., 100: 161-178.

Gribble R.F., Stern R.J., Newman S., Bloomer S.H. and O'Hearn T., 1998. Chemical and isotopic composition of lavas from the Northern Mariana Trough: implications for magma genesis in back-arc-arc basins. J. Petrol., 39: 125-154.

Ishizuka H., Kawanobe Y. and Saka H., 1990. Petrology and geochemistry of volcanic rocks dredged from the Okinawa Trough, an active back-arc basin. Geochem. J., 24: 75-92.

Jacobshagen V., Durr S., Kockel F., Kopp K.O. and Kowalczyk G., 1978. Structure and geodynamic evolution of the Aegean region. In: H. Closs, D.H. Roeder and K. Schmidt (Eds.), Alps, Apennines, Hellenides. Schweitzerbart, Stuttgart, p. 537-564.

Jones G. and Robertson A.H.F., 1991. Tectono-stratigraphy and evolution of the Pindos ophiolite and related units, northwestern Greece. J. Geol. Soc. London, 148: 267-288.

Lachance G.R. and Trail R.J., 1966. Practical solution to the matrix problem in X-ray analysis. Can. Spectr., 11: 43-48.

Kodra A., Gjata K. and Xhomo A., 2000. Tectonic history of Mirdita oceanic basin. Bul. Shkencave Gjeol., Tirana, 17 (1): 5-26.

Maillet P., Ruellan E., Gérard M., Person A., Bellon H., Cotton J., Joron J.-L., Nakada S. and Price R.C., 1995. Tectonics, magmatism, and evolution of the New Hebrides backarc troughs

(Southwest Pacific). In: B. Taylor (Ed.), Backarc basins, tectonics and magmatism, Plenum Press, New York, p. 177-235.

McKenzie D. and O'Nions R.K., 1991. Partial melt distributions from inversion of rare earth element concentrations. J. Petrol., 32: 1021-1091.

Mercier J., 1966. Mouvements orogéniques et magmatisme d'age Jurassique Supérieur-Éocrétacé dans les Zones Internes des Hellénides (Macédoine, Grèce). Rev. Géogr. Phys. Géol. Dynam., 8: 265-278.

Mercier J., Vergély P. and Bébien J., 1975. Les ophiolites hellénique «obductées» au Jurassique supérieur sont elles les vestiges d'un Océan téthysien ou d'une mer marginale péri-européene? C. R. Somm. Soc. Géol. France, 17: 108-112.

Michard A., Feinberg H. and Montigny R., 1998. Supra-ophiolitic formations from the Thessaloniki Nappe (Greece) and associated magmatism; an intra-oceanic subduction predates the Vardar obduction. C. R. Acad. Sci. Paris, Serie II, 327 (7): 493-499.

Michard A., Whitechurch H., Ricou L.E., Montigny R. and Yazgan E., 1984. Tauric subduction (Malatya-Elazig provinces) and its bearing on tectonics of the Tethyan realm in Turkey. In: J.E. Dixon and A.H.F. Robertson (Eds.), The geological evolution of the Eastern Mediterranean. Geol. Soc. London, Spec. Publ., 17: 349-360.

Miyashiro A., 1974. Volcanic rock series in island arcs and active continental margins. Am. J. Sci., 274: 321-355.

Mountrakis D., 1984. Structural evolution of the Pelagonian Zone in Northwestern Macedonia, Greece. In: J.E. Dixon and A.H.F. Robertson (Eds.), The geological evolution of the Eastern Mediterranean. Geol. Soc. London Spec. Publ., 17: 518-590.

Murton B.J., 1989. Tectonic controls on boninite genesis. In: A.D. Saunders and M.J. Norry (Eds.), Magmatism in the ocean basins. Geol. Soc. London Spec. Publ. 42: 347-377.

Pamić J., Tomljenović B. and Balen D., 2002. Geodynamic and petrogenetic evolution of Alpine ophiolites from the central and NW Dinarides: an overview. Lithos, 65: 113-142.

Papanikolaou D.J., 1984. The three metamorphic belts of Hellenides: a review and a kinematic interpretation. In: J.E. Dixon and A.H.F.Robertson (Eds.), The geological evolution of the Eastern Mediterranean. Geol. Soc. London Spec. Publ., 17: 551-561.

Pearce J.A., 1982. Trace element characteristics of lavas from destructive plate boundaries. In: R.S. Thorpe (Ed.), Andesites. Wiley, New York, p. 525-548.

Pearce J.A., 1983. Role of the sub-continental lithosphere in magma genesis at active continental margin. In: C.J. Hawkesworth and M.J. Norry (Eds.), Continental basalts and mantle xenoliths, Shiva Publ., Nantwich, p. 230-249.

Pearce J.A. and Norry M.J., 1979. Petrogenetic implications of Ti, Zr, Y, and Nb variations in volcanic rocks. Contrib. Mineral. Petrol., 69: 33-47.

Pe-Piper G. and Piper D.J.W., 2002. The igneous rocks of Greece. The anatomy of an orogen. Gebrueder Borntraeger, Berlin, 573 pp.

Ricou L.E. and Godfriaux I., 1991. Une coupe à travers les ophiolites et gneiss allochtones entre le massif Pélagonien et la fenêtre du Païkon (Grèce du Nord). C. R. Acad. Sci. Paris, 313: 1595-1601.

Robertson A.H.F., Clift P.D., Degnan P.J. and Jones G., 1991. Palaeogeographical and palaeotectonic evolution of the eastern Mediterranean Neotethys. Palaeo. Palaeo. Palaeo., 87: 289-343.

Robertson A.H.F. and Dixon J.E., 1984. Introduction: aspects of the geological evolution of the eastern Mediterranean. In: J.E. Dixon and A.H.F. Robertson (Eds.), The geological evolution of the Eastern Mediterranean, Geol. Soc. London Spec. Publ., 17: 1-74.

Robertson A.H.F., Dixon J.E., Brown S., Collins A., Morris A., Pickett E., Sharp I. and Ustaomer T., 1996. Alternative tectonic models for the Late Palaeozoic-Early Tertiary development of Tethys in the Eastern Mediterranean region. In: A. Morris and D.H. Tarling (Eds.), Palaeomagnetism and tectonics of the Mediterranean Region. Geol. Soc. London Spec. Publ., 105: 239-263.

Robertson A.H.F., Karamata S. and Resimic-Sariç K., 2008. Introduction: Role of ophiolites and related units in the Late Palaezoic-Early Cenozoic tectonic development of Tethys in the northern Balkan Peninsula. In: A.H.F. Robertson, S. Karamata and K. Resimic-Sariç (Eds.), Balkan ophiolites, Lithos, Spec. Publ., in press.

Robertson A.H.F.. and Shallo M., 2000. Mesozoic - Tertiary tectonic evolution of Albania in its regional Eastern Mediterranean context. Tectonophysics, 316: 197-214.

Ross J.V. and Zimmerman J., 1996. Comparison of evolution and tectonic significance of the Pindos and Vourinos ophiolite suite, northern Greece. Tectonophysics, 256: 1-15.

Saccani E., Beccaluva L., Coltorti M. and Siena F., 2004. Petrogenesis and tectono-magmatic significance of the Albanide-Hellenide ophiolites. Ofioliti, 29: 77-95.

Saccani E., Padoa E. and Photiades A., 2003. Triassic mid-ocean ridge basalts from the Argolis Peninsula (Greece): new constraints for the early oceanization phases of the Neo-Tethyan Pindos basin. In: Y. Dilek and P.T. Robinson (Eds.), Ophiolites in earth history. Geol. Soc. London Spec. Publ., 218: 109-127.

Saccani E., Photiades A., Santato A. and Zeda O., 2008. New evidence for supra-subduction zone ophiolites in the Vardar Zone from the Vermion Massif (northern Greece): Implication for the tectono-magmatic evolution of the Vardar oceanic basin. Ofioliti, 33: 17-37.

Sariç K., Cvetkoviç V., Romer R.L., Christofides G. and Koroneos A., 2008. Granitoids associated with East Vardar ophiolites (Serbia, F.Y.R. of Macedonia and northern Greece): Origin, evolution and geodynamic significance inferred from major and trace element data and Sr-Nd-Pb isotopes. Lithos, doi:10.1016/j.lithos.2008.06.001.

Saunders A.D. and Tarney J., 1979. The geochemistry of basalts from a back-arc spreading centre in the East Scotia Sea. Geochim. Cosmochim. Acta, 43: 555-572.

Schermer E.R., 1993. Geometry and kinematics of continental basement deformation during the Alpine Orogeny, Mt Olympos, Greece. J. Struct. Geol., 15: 571-591.

Şengör A.M.C. and Yılmaz Y., 1981. Tethyan evolution of Turkey: a plate tectonic approach. Tectonophysics, 75: 181-241.

Serri G., 1981. The petrochemistry of ophiolite gabbroic complexes: a key for the classification of ophiolites into low-Ti and high-Ti types. Earth Planet. Sci. Lett., 52: 203-212.

Shallo M., 1992. Geological evolution of the Albanian ophiolites and their platform periphery. Geol. Runds., 81: 681-694.

Sharp I. and Robertson A., 1994. Late Jurassic - Lower Cretaceous oceanic crust and sediments of the eastern Almopias Zone, NW Macedonia (Greece); implications for the evolution of the eastern "Internal" Hellenides. Bull. Geol. Soc. Greece, 30: 47-61.

Sharp I.R. and Robertson A.H.F., 2006. Tectonic-sedimentary evolution of the western margin of the Mesozoic Vardar Ocean: evidence from the Pelagonian and Almopias zones, northern Greece. In: A.H.F. Robertson and D. Mountrakis (Eds.), Tectonic development of the Eastern Mediterranean Region. Geol. Soc. London Spec. Publ., 260: 373-412.

Shervais J.W., 1982. Ti-V plots and the petrogenesis of modern ophiolitic lavas. Earth Planet. Sci. Lett., 59: 101-118.

Smith A.G., 2006. Tethyan ophiolite emplacement, Africa to Europe motions, and Atlantic spreading. In: A.H.F. Robertson and D. Mountrakis (Eds.), Tectonic development of the Eastern Mediterranean Region. Geol. Soc. London Spec. Publ., 260: 11-34.

Spray J.G., Bébien J., Rex D.C. and Roddick J.C., 1984. Age constraints on the igneous and metamorphic evolution of the Hellenic-Dinaric ophiolites. In: J.E. Dixon and A.H.F. Robertson (Eds.), The geological evolution of the Eastern Mediterranean. Geol. Soc. London Spec. Publ., 17: 619-627.

Stais A., Ferrière J., Caridroit M., De Wever P., Clement B. and Bertrand J., 1990. Données nouvelles sur l'histoire ante-obduction (Trias-Jurassique) du domaine d'Almopias (Macédoine, Grèce). C. R. Acad. Sci. Paris, Serie II, 310: 1275-1480.

Stampfli G.M. and Borel G.D., 2002. A plate tectonic model for the Paleozoic and Mesozoic constrained by dynamic plate

boundaries and restored synthetic oceanic isochrons. Earth Planet. Sci. Lett., 196: 17-33.

Sun S.S. and McDonough W.F., 1989. Chemical and isotopic systematics of ocean basalts: Implications for mantle composition and processes. In: A.D. Saunders and M.J.Norry (Eds.), Magmatism in the ocean basins. Geol. Soc. London Spec. Publ., 42: 313-346.

Vergély P., 1976. Origine "vardarienne" chevauchement ver l'ouest et rétrocharriage vers l'est des ophiolites de Macedoine (Grèce) au cours du Jurassique supérieur-Eocrétace. C. R. Acad. Sci. Paris, D280: 1063-1066.

Vergély P., 1984. Tectonique des ophiolites dans les Hellenides internes (déformations, métamorphismes et phénomènes sédimentaires): consequences sur l'evolution des regions Tethysiennes occidentales. These d'Etat, Univ. Paris-Sud, 611 pp.

Vergély P. and Mercier J.-L., 2000. Données nouvelles sur les chevauchements d'âge post-Crétacé supérieur dans le massif du Paikon (zone de l'Axios-Vardar, Macédoine, Grèce): un nouveau modèle structural. C. R. Acad. Sci. Paris, Series IIA, 330: 555-561.

Volpe A.M., Macdougall J.D. and Hawkins J.W., 1987. Mariana Trough basalts (MTB): trace element and Sr-Nd isotopic evidence for mixing between MORB-like and Arc-like melts. Earth Planet. Sci. Lett., 82: 241-254.

Weaver S.D., Saunders A.D., Pankhurst R.J. and Tarney J., 1979. A geochemical study of magmatism associated with the initial stages of back-arc spreading: the Quaternary volcanics of Bransfield Strait, from South Shetland Islands. Contrib. Mineral. Petrol., 68: 151-169.

Wood D.A., Marsh N.G., Tarney J., Joron J.L., Fryer P. and Treuil M., 1982. Geochemistry of igneous rocks recovered from a transect across the Mariana Trough, arc, fore-arc, and trench, sites 453 through 461, Deep Sea Drilling Project Leg 60. D.S.D.P. Initial Rep., 60: 611-645.

Zachariadis P., Kostopoulos D., Reischmann T., Himmerkus F., Matukov D. and Sergeev S., 2006. U-Pb ion-microprobe zircon dating of subduction-related magmatism from northern Greece: The ages of the Guevgueli, Thessaloniki and Chalkidiki igneous complexes. Geophys. Res. Abstr., 8: SRef-ID: 1607-7962/gra/EGU06-A-05560.

Zachariadou S. and Dimitriadis S., 1995. Aspects of the tectonomagmatic evolution of the Late Jurassic Guevgueli Complex, Macedonia, Greece. Geol. Soc. Greece Spec. Publ., 4: 143-147.

Zimmerman J., 1972. Emplacement of the Vourinos ophiolitic complex, northern Greece. Geol. Soc. Am. Mem, 132: 225-239.

Received, march 19, 2008
Accepted, November 4, 2008